

STUDY ON SOFT-FINGERED HANDLING VIA
MINIMUM DOF ROBOTIC HAND FOR ROBUST
MANIPULATION

DOCTORAL PROGRAM IN SCIENCE AND ENGINEERING
GRADUATE SCHOOL OF SCIENCE AND ENGINEERING
RITSUMEIKAN UNIVERSITY

Takahiro Inoue
November 2006

© Copyright by Takahiro Inoue 2006
All Rights Reserved

I certify that I have read this thesis and that, in my opinion, it is fully adequate in scope and quality as a thesis for the degree of Doctor.

Shinichi Hirai
(Principal Adviser)

I certify that I have read this thesis and that, in my opinion, it is fully adequate in scope and quality as a thesis for the degree of Doctor.

Suguru Arimoto

I certify that I have read this thesis and that, in my opinion, it is fully adequate in scope and quality as a thesis for the degree of Doctor.

Naoki Takano

Approved for the University Committee on Graduate Studies.

Preface

My intension in writting this doctoral dissertation is to widely announce my research field, in which certain kinds of basic mathematical and physical concept associated with soft materials and soft-fingered handling issue are mentioned. We mapped down in relation to the process of deriving a number of equations, integral calculations etc. so that everybody can easily understand our theory derived in this dissertation. This dissertation tells you all you need to know about handling systems with soft fingertips, especially reveal contact mechanics between the fingertips and a target object grasped by a robotic hand. It will become very obvious that our study is a significant newest research over your deep reading, and you will have a deep interest in our contact model of soft fingertip and the mechanisms of secure soft-fingered manipulation.

This study relating to the contact model of soft fingertip have just started in April, 2002. All the fruits of the study are written in this paper. First, we have started our study by producing a small soft fingertip that suits for robotic fingers, and an one-dimensional contact model of the fingertip is mentioned in Chapter 2. An important finding that a local minimum point of elastic potential energy exists on the fingertip deformation is newly proposed. Readers can understand that the local minimum of elastic potential energy (LMEE) plays a significant role in secure grasping and robust manipulation by soft fingers.

In Chapter 3, we formulate an extended fingertip model that includes not only geometrical nonlinearity of the hemispherical shape, but also material nonlinearity of the fingertip material. This gives pretty good results in terms of load-compression test of the hemispherical fingertip up to large deformation.

In Chapter 4, we first give an extended LMEE that contains elastic energy generated on two soft fingers of a minimum degrees of freedom robotic hand. By representing four

kinds of geometrical constraints that appear on the soft-fingered handling, we show that the LMEE with the constraints converges to a certain point, that is, stable grasping and robust manipulation are steadily achieved even in the two degrees of freedom robotic hand.

In Chapter 5, we remodel our one-dimensional fingertip model to an extended two-dimensional model, in which the bending motion of the fingertip along lateral direction is also included into the remodeling. Furthermore, we represent the constraints mentioned in Chapter 4 more rigorously, where tangential constraints for the object surface is given by nonholonomic constraints that include the infinitesimal bending motion. In order to solve the equations of motion of the handling system and show the dynamic behavior of the grasped object, we apply the Constraint Stabilization Method (CSM) to the numerical analysis of the dynamic simulation, in which both holonomic and nonholonomic constraints are included. Finally, we clarify that the stable grasping and robust manipulation by soft-fingered hand are able to consistently be achieved easily without any object information during the manipulation.

We hope that all readers will comprehend our research and take a step in these kind of study : object manipulation by means of soft fingered robotic hand.

Takahiro Inoue

September 25, 2006

Acknowledgements

I would like to thank my principal adviser, Prof. Shinichi Hirai. When I came to Ritsumeikan University in 2002, he gave me immediately a newest topic where nobody have ever taken a step in. He consistently gave me stimulating discussion about our newest study anytime and anywhere. As a result, totally my seven papers have fortunately been accepted for only four years on *IEEE Int. Conf. Intelligent Robots and Systems*, *IEEE Int. Conf. Robotics and Automation*, and *ISER 2006*. Again, "Thank you for a great deal of advice and suggestion".

Also I appreciate having the opportunity to meet all members of Hirai laboratory and also a secretary, Mrs. Hatanaka. She often helps me make some documents or something like that. I hope that they all will facilitate their studies and achieve their objectives in near future. Also I really thank my wife "Mayumi" and my first baby "Kouki". I hope eternal and continuous happy days will keep on coming to our family, and forever...

Contents

| | |
|--|-----------|
| Preface | iv |
| Acknowledgements | vi |
| 1 Introduction | 1 |
| 1.1 Fingertip Deformation Model | 1 |
| 1.2 Quasi-static Manipulation Analysis | 3 |
| 2 Geometrical Nonlinear Elastic Model | 6 |
| 2.1 Measurement of Young's Modulus | 6 |
| 2.2 Fingertip Stiffness | 9 |
| 2.3 Elastic Force | 11 |
| 2.4 Elastic Potential Energy | 12 |
| 2.5 Compression Test of a Hemispherical Soft Fingertip | 13 |
| 2.6 Concluding Remarks | 17 |
| 3 Geometrical and Material Nonlinear Elastic Model | 18 |
| 3.1 Hertzian Contact and Kao's Elastic Model | 19 |
| 3.2 Identification of Nonlinear Young's Modulus | 19 |
| 3.3 Comparison with Hertzian Contact | 22 |
| 3.4 Force Comparison | 23 |
| 3.5 Concluding Remarks | 26 |

| | | |
|----------|--|-----------|
| 4 | Quasi-Static Manipulation with Soft Fingers | 27 |
| 4.1 | Geometric Constraints | 27 |
| 4.1.1 | Normal Constraints | 28 |
| 4.1.2 | Tangential Constraints | 30 |
| 4.2 | Quasi-Static Manipulation | 33 |
| 4.2.1 | Algorithm Using Extended LMEE | 33 |
| 4.2.2 | Method of Numerical Analysis | 34 |
| 4.3 | Simulation | 35 |
| 4.4 | Experiments | 36 |
| 4.4.1 | Apparatus and Parameters | 37 |
| 4.4.2 | Experimental Method | 37 |
| 4.4.3 | Experimental Results | 38 |
| 4.5 | Concluding Remarks | 42 |
| 5 | Dynamic Manipulation with Soft Fingers | 44 |
| 5.1 | Two-dimensional Elastic Model of Soft Fingertip | 45 |
| 5.2 | Holonomic and Nonholonomic Constraints | 46 |
| 5.2.1 | Normal Constraints | 46 |
| 5.2.2 | Tangential Constraints | 48 |
| 5.3 | General Description of Equations of Motion | 49 |
| 5.3.1 | Lagrangian | 49 |
| 5.3.2 | Equations of Motion | 50 |
| 5.3.3 | Constraint Stabilization Method including Nonholonomic Constraints | 50 |
| 5.4 | E.O.Ms for Dynamic Manipulation | 51 |
| 5.4.1 | Constraint Matrix | 52 |
| 5.4.2 | Equations of Motion | 53 |
| 5.5 | Simulation | 54 |
| 5.5.1 | Example Motion | 54 |
| 5.5.2 | Results | 56 |
| 5.6 | Concluding Remarks | 56 |
| 6 | Conclusions | 60 |

| | |
|--|-----------|
| A Contact Plane Formula | 61 |
| B Spring Constant Formulation | 62 |
| C Coordinate Conversion to Derive the Fingertip Stiffness | 64 |
| D Relationship between Elastic Force and Potential Energy | 67 |
| E Approximation Method for Nonlinear Curve | 69 |
| Bibliography | 71 |

List of Tables

| | | |
|-----|---------------------------------------|----|
| 4.1 | System parameters | 37 |
| 5.1 | Simulation parameters | 55 |
| E.1 | Asymptotical standard error | 70 |

List of Figures

| | | |
|------|--|----|
| 2.1 | Contact mechanism | 7 |
| 2.2 | Compression test of a hemispherical soft fingertip. | 8 |
| 2.3 | Stress-strain diagram of polyurethane rubber. | 8 |
| 2.4 | Average value of stress-strain diagram. | 8 |
| 2.5 | Integration area. | 10 |
| 2.6 | Comparison between numerical results of Eq. (2.3) and analytical simulations of Eq. (2.7) when $E = 0.2032$ MPa. | 10 |
| 2.7 | Comparison between the numerical integration and the analytical simulation of F and P , respectively. | 13 |
| 2.8 | Elastic forces in experiments. | 15 |
| 2.9 | Simulation results of elastic force. | 16 |
| 2.10 | Experimental results of elastic force. | 16 |
| 2.11 | Local minimum of elastic force. | 16 |
| 3.1 | Cylindrical specimens | 20 |
| 3.2 | Stress strain diagram | 20 |
| 3.3 | Comparison between the material nonlinear elastic force model and conventional force models (Eq. (2.11) and Hertzian model) when $\theta_p = 0$ and $E = 0.232$ [MPa]. | 23 |
| 3.4 | Comparison between elastic forces in geometrical and material nonlinear model. | 24 |
| 3.5 | Comparison between simulations and experiments | 25 |
| 3.6 | Local minimum of elastic forces | 25 |

| | | |
|-----|---|----|
| 4.1 | Soft-fingered manipulation | 28 |
| 4.2 | Normal constraints | 29 |
| 4.3 | Tangential constraints | 30 |
| 4.4 | Passive rolling | 32 |
| 4.5 | Quasi-static manipulation process | 36 |
| 4.6 | Apparatus | 38 |
| 4.7 | Binary images | 39 |
| 4.8 | Comparison with simulation and experiment | 41 |
| 4.9 | Comparison of object position in experiments | 42 |
| 5.1 | Contact mechanism during the soft-fingered manipulation | 45 |
| 5.2 | Soft-fingered manipulation under the gravitational force | 47 |
| 5.3 | Geometric relationship between grasped object and both fingertips | 47 |
| 5.4 | Snapshots on simulation | 54 |
| 5.5 | Simulation results of object position and orientation | 57 |
| 5.6 | Convergence of four constraints | 58 |
| B.1 | Spring constant inside the soft fingertip. | 63 |
| C.1 | Equivalent fingertip stiffness with respect to Σ'' -coordinate system. | 65 |
| C.2 | Fingertip stiffness on a certain perimeter. | 66 |

Chapter 1

Introduction

1.1 Fingertip Deformation Model

To date, various research has been done on manipulations of objects by soft-fingered robotic hands. Most of the studies, particularly earlier studies, focused only on contact mechanisms on various soft fingers. More recently, there has been an increase in studies on sensing mechanisms of human hand and designing control systems in robotic applications to emulate the human capabilities which are applicable to robotic hands. The conventional studies, however, have not been explicitly providing any analytical exploration of the simplicity in grasping and manipulating motions in terms of the soft-fingered handling. As a cause of the above mention, it has been substantially difficult to derive a fine elastic model of soft materials used in the fingertips.

Yokokohji *et al.* proposed a control scheme with visual sensors which can cancel the frictional twist/spin moment at the contact point of soft fingertips, and achieved stable grasping by spherical soft fingertips [1, 2]. Maekawa *et al.* developed a finger-shaped tactile sensor covered with a soft and thin material, and proposed a control algorithm based on tactile feedback using the sensor, which needs no information about the geometry of the grasped object [3, 4]. They managed to control the position of an object along a desired trajectory. In these papers, point-contacts were used to represent constraints of rolling contact in their theoretical models, although the fingertips were made from soft material such as rubber. Arimoto *et al.* verified the passivity of equations of motion for a total

handling system by using a Lagrangian function incorporating the elastic potential energy due to the deformation of soft fingertips [5], and compensated for the gravity effect in three-dimensional space [6]. An elastic force model was also derived for the elastic potential energy of a system in which virtual linear springs were arranged for simplicity in a radial pattern inside hemispherical soft fingertips. Doulgeri *et al.* discussed the problem of stable grasping with deformable fingertips on which rolling constraints were described as non-holonomic because of change in the effective rolling radius of the soft fingertip [7, 8]. The above studies, however, focused mainly on deriving a control law to realize stable grasping and pose control of the grasped object, not on revealing a physically appropriate deformation model, which also contains the nonlinear characteristics of a hemispherical soft fingertip.

On the other hand, Xydas *et al.* proposed an exact deformation model based on the mechanics of the materials containing nonlinear characteristics, and performed Finite Element (FE) analysis for a hemispherical soft fingertip [9, 10]. Kao *et al.* experimentally demonstrated that the elastic force due to deformation satisfied a power law with respect to the displacement of the fingertip, and insisted that their theory subsumes Hertzian contact [11]. These studies, however, did not distinguish between the material nonlinearity of the soft fingertip and the geometrical nonlinearity caused by the hemispherical shape of the fingertip, and defined a parameter including the effect of both nonlinearities. Consequently, the cause of the discrepancy between the results of the simulation based on their model and the results of actual experiments was not apparent. In addition, because of the complexity of their proposed models, these studies do not lend themselves to analysis of equations of motion for the soft-fingered manipulation system overall. While FE analysis may enable us to derive a stress distribution and an elastic force on the soft fingertip, these simulation results depend on the selected mesh pattern. Although FE analysis based on a certain arbitrary mesh pattern may prove the stability for equations of motion of the handling system, it does not always provide proof of stability for equations derived from other mesh patterns.

In this report, especially in Chapter 2, we propose a static elastic model of a hemispherical soft fingertip in a physically reasonable and straightforward form suitable for theoretical analysis of robotic handling motions [12, 13]. We distinguish between geometric nonlinearity due to the hemispherical shape and material nonlinearity of soft materials, i.e., the

nonlinearity of the Young's modulus of the soft material, allowing us to focus only on the geometric nonlinearity of the soft fingertip, and analytically formulate elastic force and elastic potential energy equations for the deformation of the fingertip. We show that each formula is a function of two variables: the maximum displacement of the fingertip and the orientation angle of a contacting object. We also show that when the object is positioned normal to the fingertips, the elastic potential energy is minimum. We finally validate the static elastic model by conducting a compression test of the hemispherical soft fingertip and comparing the results.

In addition, in Chapter 3 we formulate an improved elastic force model including not only the geometrical nonlinearity but also the material nonlinearity in the modeling. We newly define a nonlinear Young's modulus that is useful for simplifying the static analysis of the soft fingertip. We show that the new elastic force model gives pretty good results on the compression test of a hemispherical soft fingertip.

1.2 Quasi-static Manipulation Analysis

Almost all studies on grasping of objects have assumed that the robot's fingertip is rigid and that it is point-contact with the object, hence it relatively simplifies mathematical descriptions [14–16]. Since the grasped object moves and rolls without any change of the rolling radius in the case of rigid point-contact model, it is comparatively easy to analytically describe equations of motion of whole handling system based on geometrical relationships.

Humans can grasp and manipulate an object in a relatively easy way by using their soft fingers, and achieve position and force controls of the grasped object by feeding back informations obtained from their visual and tactile sensings. In the strive to achieve grasping capabilities as good as human's, we need to model soft fingertips because they are much better than hard fingertips at grasping since they usually form a larger area in contact with the object, and we need to design control schemes for soft-fingered robotic hand which is necessary to realize versatile and sophisticated motions of human hand.

Xydas *et al.* [9, 10] and Kao *et al.* [11] performed FE analysis to describe an exact deformation model of a hemispherical soft fingertip, but the model was limited to only vertical contact deformation of the soft fingertip, making it impossible to apply their model

to derive equations of motion for the overall handling system and to analytically discuss stability. Nguyen *et al.* [17] proposed a simple deformation model of a soft fingertip in order to derive an appropriate control law for a multi-fingered robotic hand. The deformation model, however, assumes that all the elastic forces acting on the soft fingertip face toward the origin of the fingertip in a radial-directional pattern. Therefore, it is difficult to physically represent the contact model of the fingertip and equations of motion of the object relating to the plane-contact. Yokokohji *et al.* [2] used a CCD camera for visual feedback to a three-fingered robotic hand grasping an object. Although the fingers were soft, in their mathematical model, they applied conventional point-contact theory and derived equations of motion with rolling constraints that are applicable to rigid fingertips. Arimoto *et al.* [5, 18] defined an elastic force equation based on the above radial-directional model, and demonstrated the passivity of a dynamic robotic hand system with soft fingertips. Doulgeri *et al.* [7, 8] derived equations of motion for a soft-fingered manipulation system, and proposed a control law for the pinching motion of a grasped object by considering non-holonomic constraints that stem from the rolling velocity of the object. Fasoulas *et al.* introduced a rolling factor dependent on the material of a deformable fingertip, and showed that the input torque was directly related to fingertip deformation and the rolling factor by deriving equilibrium conditions obtained from the static force/moment balance between the grasped rigid object and two fingertips [19]. The above studies, however, used a simple radial-directional model to find an attractive control law, but because the elastic force was assumed to be constant in the model, the control law tended to become complicated.

In Chapter 4, therefore, we focus on the potential energy associated with large deformation of a hemispherical soft fingertip used in two-fingered hand, and show that the extended elastic potential energy formula has a local minimum and it plays important role in the stable grasping and robust manipulation by soft-fingered robotic hand. Based on the above mentions, we propose a new quasi-static manipulation methodology using the LMEE numerical algorithm via two-fingered robotic hand with minimum degrees of freedom [20, 21]. We demonstrate that the quasi-static manipulation theory is able to determine unique position and orientation of the manipulated object by the soft-fingered hand.

In addition, in Chapter 5 we first improve the one-dimensional fingertip model to a two-dimensional model by adding the bending motion of the fingertip to the conventional

motion in which simple compression is only considered. Furthermore, we clarify non-holonomic constraints induced by the soft-fingered manipulation, which is represented as a velocity-form constraint. We apply the Constraint Stabilization Method (CSM) that contains both holonomic and nonholonomic constraints at one time to the soft-fingered handling system in order to analyze the dynamic behavior of a grasped object by means of minimum degrees of freedom soft-fingered hand.

Chapter 2

Geometrical Nonlinear Elastic Model

In this chapter, we derive an elastic force and potential energy formula in a straightforward form, which are applicable to the analysis of grasping and manipulating motion by two-fingered robotic hand. We treat the fingertips as if they were composed of an infinite number of virtual linear springs standing vertically. Figure 2.1 shows one such spring. We formulate elastic force and elastic potential energy equations for the deformation of the fingertip. In order to simplify the derivation process of both equations, two assumptions associated with material characteristics are given as follows:

1. The incompressibility of elastomer materials is not dealt with.
2. Young's modulus is constant.

Note that the contact condition being discussed in the present study is restricted to the case that an applied force to the fingertip is assumed to be along z -axis of the fingertip. In addition, we consider that an object never comes into contact with the underneath plane of the fingertip.

2.1 Measurement of Young's Modulus

In the present study, the Young's modulus of the soft fingertip was measured by conducting a compression test on 6 cylinders of polyurethane gel, as shown in Figure 2.2-(a). Three

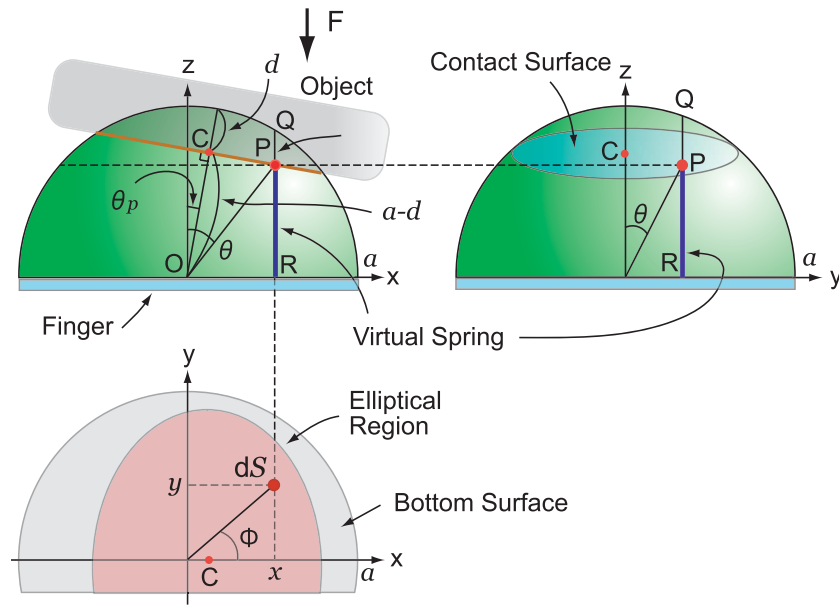


Figure 2.1: Contact mechanism

cylinders were 20 mm in diameter and 15, 20, and 25 mm in height, and three were 30 mm in diameter and also 15, 20, and 25 mm in height, as shown in Figure 2.2-(b).

Figure 2.3-(a) shows the overall view of a measured stress-strain diagram, and an enlarged view of part of the diagram is shown in Figure 2.3-(b). Numerical values shown in both graphs denote the specimen height on the left side and the specimen diameter on the right side. The data were averaged and smoothed using the least-squares method (LSM), as shown in Figure 2.4. We assumed that the maximum deformation of the soft fingertip is 50% in the radius. Furthermore, in order to focus predominantly on the geometric nonlinearity due to the hemispherical shape, we avoided the issue of the material's nonlinearity which is directly related to the Young's modulus of soft materials. Consequently, we performed a linear approximation for a 50% strain, as in Figure 2.4, and estimated the Young's modulus as 0.2032 MPa.

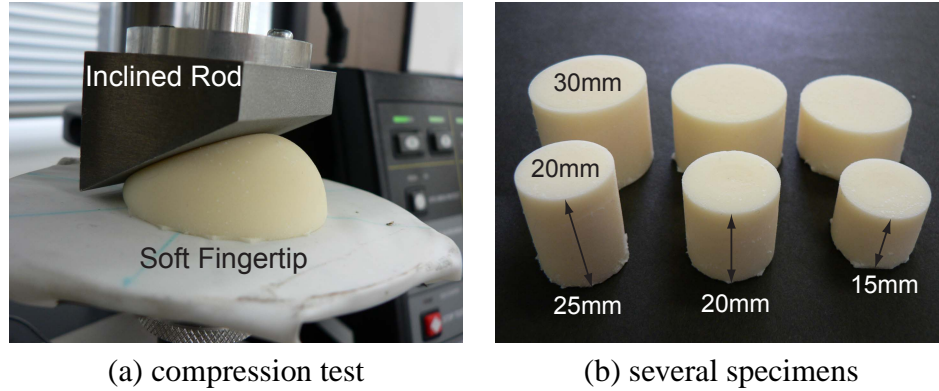


Figure 2.2: Compression test of a hemispherical soft fingertip.

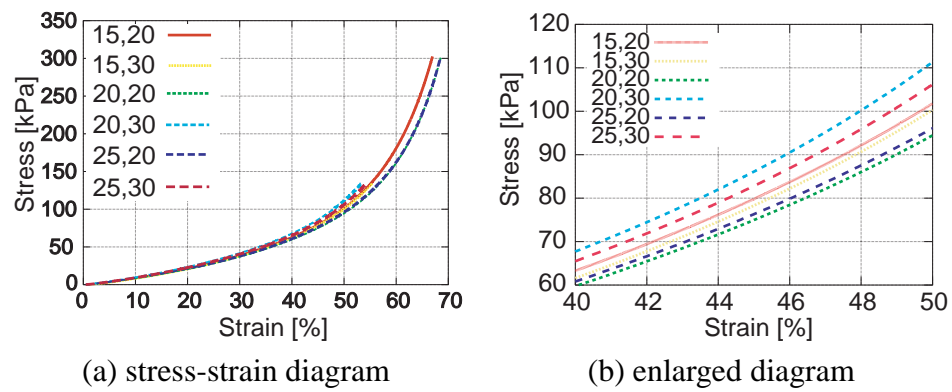


Figure 2.3: Stress-strain diagram of polyurethane rubber.

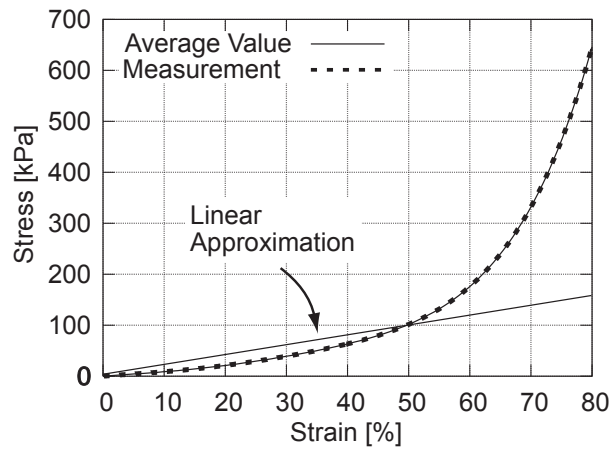


Figure 2.4: Average value of stress-strain diagram.

2.2 Fingertip Stiffness

Let us apply an infinitesimal virtual spring QR with sectional area dS inside the soft fingertip, as shown in Figure 2.1. Let dF be the infinitesimal elastic force due to the shrinkage PQ of the virtual spring. Let θ_p be the orientation angle of the contacting object, a be the fingertip radius, d be the maximum displacement of the fingertip, $a_c = \sqrt{a^2 - (a-d)^2}$ be the radius of the contacting circle, and P be the point where the spring is in contact with the object. Furthermore, let θ be the angle subtended between line PQ and the z -axis, and ϕ be the azimuthal angle on the xy -plane. Using the contact surface equation, $x \sin \theta_p + z \cos \theta_p = a - d$ (see Appendix A), the infinitesimal elastic force dF is

$$dF = k \cdot PQ = k \left\{ \sqrt{a^2 - (x^2 + y^2)} - \frac{a - d - x \cdot \sin \theta_p}{\cos \theta_p} \right\}, \quad (2.1)$$

where k is the spring constant of the spring QR . Note that k is proportional to the sectional area dS and inversely proportional to the natural length $\sqrt{a^2 - (x^2 + y^2)}$. Letting E be the Young's modulus of soft finger materials, k is described as (see Appendix B)

$$k = \frac{E dS}{\sqrt{a^2 - (x^2 + y^2)}}. \quad (2.2)$$

Letting K be the fingertip stiffness on the entire deformed part illustrated in Figure 2.1, K can be expressed from Eq. (2.2) as

$$K = \int_{ell} k = E \int_{-a_c}^{a_c} \int_{b_1(y)}^{b_2(y)} \frac{dx dy}{\sqrt{a^2 - (x^2 + y^2)}}, \quad (2.3)$$

where

$$b_1(y) = (a - d) \sin \theta_p - \cos \theta_p \sqrt{a_c^2 - y^2}, \quad (2.4)$$

$$b_2(y) = (a - d) \sin \theta_p + \cos \theta_p \sqrt{a_c^2 - y^2}, \quad (2.5)$$

and ell denotes the elliptical region shown in Figure 2.5. Applying a numerical integration to Eq. (2.3), we obtain a constant fingertip stiffness depicted as continuous lines, as shown in Figure 2.6. This indicates that the fingertip stiffness K is independent of the object

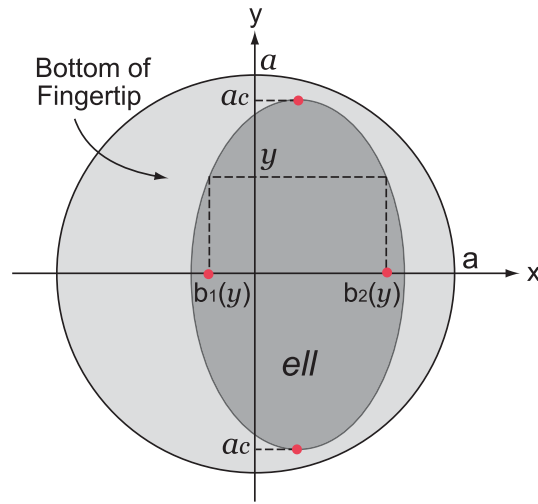


Figure 2.5: Integration area.

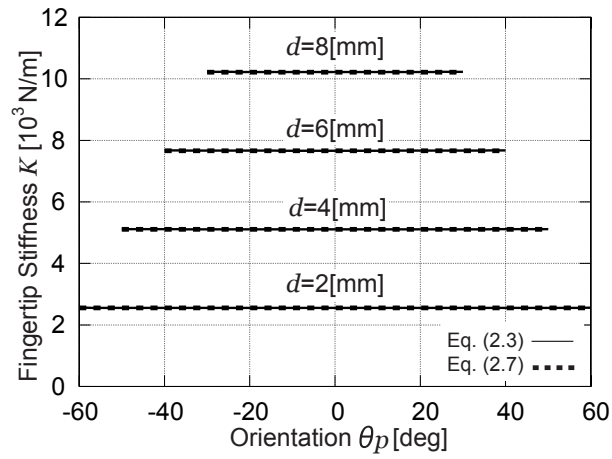


Figure 2.6: Comparison between numerical results of Eq. (2.3) and analytical simulations of Eq. (2.7) when $E = 0.2032$ MPa.

orientation θ_p . Hence, in this study we provide a third additional assumption that:

3. the fingertip stiffness is constant to the change of the object orientation.

By using the above assumption, we formulate the fingertip stiffness K in an analytical formula.

Now, performing a substitution that $x = r \cos \phi \cos \theta_p + (a - d) \sin \theta_p$ and $y = r \sin \phi$, Eq. (2.3) is then transformed into (see Appendix C)

$$K = E \int_0^{a_c} r \left\{ \int_0^{2\pi} \frac{\cos \theta_p d\phi}{\sqrt{a^2 - \{x^2(r, \phi) + y^2(r, \phi)\}}} \right\} dr. \quad (2.6)$$

Since K is independent of θ_p (assumption 3), we can substitute $\theta_p = 0$ into Eq. (2.6), and get:

$$K = E \int_0^{a_c} r \left\{ \int_0^{2\pi} \frac{d\phi}{\sqrt{a^2 - r^2}} \right\} dr = 2\pi E d. \quad (2.7)$$

Plotting the simulation result of Eq. (2.7) as dotted lines onto Figure 2.6 together with the results of Eq. (2.3), we find that both lines coincide with each other. This implies that the third assumption due to the numerical observation is appropriate, and additionally the stiffness is a function of only the maximum displacement d .

2.3 Elastic Force

Likewise, by using the third assumption associated with the fingertip stiffness, we formulate the elastic force and potential energy equations in a straightforward way. Using Eqs. (2.1), (2.2) and a geometrical relationship $QT = PQ \cos \theta_p$ (see Figure C.1), the elastic force F can be written as

$$\begin{aligned} F &= \frac{1}{\cos \theta_p} \int_{ell} k \cdot QT \\ &= \frac{E}{\cos \theta_p} \int_{-a_c}^{a_c} \int_{b_1(y)}^{b_2(y)} \frac{QT \cdot dx dy}{\sqrt{a^2 - (x^2 + y^2)}}. \end{aligned} \quad (2.8)$$

Performing the same variable conversion as the derivation process of K , Eq. (2.8) is then transformed as

$$F = \frac{E}{\cos \theta_p} \int_0^{a_c} QT(r) \cdot r \left\{ \int_0^{2\pi} B(r, \phi) d\phi \right\} dr, \quad (2.9)$$

where (see Figure C.1)

$$QT(r) = \sqrt{a^2 - r^2} - (a - d). \quad (2.10)$$

In Eq. (2.9), $B(r, \phi)$ corresponds to the integrand within the braces in Eq. (2.6). Here applying the assumption 3 to $B(r, \phi)$ as well as Eq. (2.7), F is finally be calculated as

$$F = \frac{E}{\cos \theta_p} \int_0^{a_c} QT(r) \cdot r \left\{ \int_0^{2\pi} \frac{d\phi}{\sqrt{a^2 - r^2}} \right\} dr = \frac{\pi E d^2}{\cos \theta_p}. \quad (2.11)$$

2.4 Elastic Potential Energy

As well as Eq. (2.8), the elastic potential energy P is expressed as

$$\begin{aligned} P &= \frac{1}{2} \int_{ell} k \cdot PQ^2 = \frac{1}{2 \cos^2 \theta_p} \int_{ell} k \cdot QT^2 \\ &= \frac{E}{2 \cos^2 \theta_p} \int_{-a_c}^{a_c} \int_{b_1(y)}^{b_2(y)} \frac{QT^2 \cdot dx dy}{\sqrt{a^2 - (x^2 + y^2)}}. \end{aligned} \quad (2.12)$$

Performing the same variable conversion as the derivation process of F , Eq. (2.12) is then transformed as

$$P = \frac{E}{2 \cos^2 \theta_p} \int_0^{a_c} QT^2(r) \cdot r \left\{ \int_0^{2\pi} B(r, \phi) d\phi \right\} dr. \quad (2.13)$$

Here again, applying the assumption 3 to $B(r, \phi)$ in Eq. (2.13), P is finally be calculated as

$$\begin{aligned} P &= \frac{E}{2 \cos^2 \theta_p} \int_0^{a_c} QT^2(r) \cdot r \left\{ \int_0^{2\pi} \frac{d\phi}{\sqrt{a^2 - r^2}} \right\} dr \\ &= \frac{\pi E d^3}{3 \cos^2 \theta_p}. \end{aligned} \quad (2.14)$$

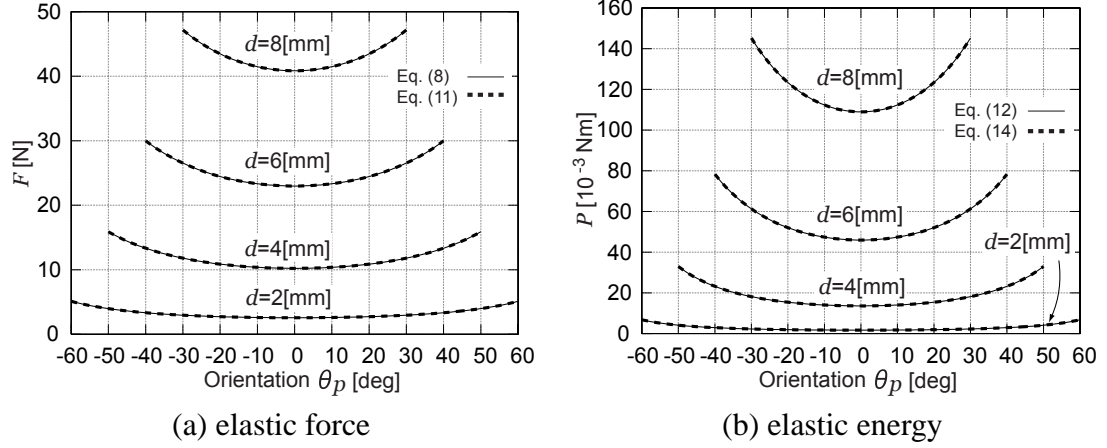


Figure 2.7: Comparison between the numerical integration and the analytical simulation of F and P , respectively.

Note that Eqs. (2.11) and (2.14) clarify that the elastic force and elastic potential energy on the entire deformed part of a hemispherical soft fingertip are functions of two variables, namely the maximum displacement d and the object orientation angle θ_p . Furthermore, we find that both formulae have a local minimum when the orientation angle is zero. Especially, we describe the minimum value of elastic energy as *Local Minimum of Elastic Potential Energy*, which is abbreviated as *LMEE*.

Finally, in order to confirm the transformations of formulae from Eq. (2.8) to Eq. (2.11) and Eq. (2.12) to Eq. (2.14), we verify the numerical analysis of Eqs. (2.8) and (2.12) and simulation results of Eqs. (2.11) and (2.14). Figure 2.7 indicates the result, and concludes that both Eqs. (2.11) and (2.14) are mathematically reasonable formulae in the present study.

Note that the elastic force obtained by differentiating Eq. (2.14) with respect to d is not identical to Eq. (2.11) (see Appendix D).

2.5 Compression Test of a Hemispherical Soft Fingertip

By compressing a hemispherical soft fingertip made of polyurethane gel along the normal direction, as shown in Figure 2.1 and Figure 2.2-(a), we verify the validity of our elastic force model represented in Eq. (2.11). Furthermore, by conducting multiple experiments

with various contacting angles, we demonstrate the existence of the local minimum of the elastic force. In the compression test, we use a fingertip with a diameter of 40 mm, and contacting rods with thirteen different shapes. The rods are inclined from 0 to 30 deg in increments of 2.5 deg, as shown in Figure 2.2-(a). Figure 2.8 compares experiments with simulation results. The horizontal axis represents the maximum displacement of the compressed fingertip, while the vertical axis represents the elastic force measured by a loadcell placed in the compression machine.

In all the graphs in Figure 2.8, the simulation and experimental results are almost identical to each other up to $d = 6.0$ mm, after which the discrepancies increase with the magnitude of the displacement. The discrepancy comes from the linear approximation of the experimental stress-strain diagram shown in Figure 2.4. The effect leads directly to nonlinearity of Young's modulus, which is outside the scope of the present Chapter.

Figure 2.9-(a) and Figure 2.10-(a) show simulation and experimental results, respectively. Enlarged views of both results are also shown in Figure 2.9-(b) and Figure 2.10-(b). The numerical values in each graph denote the inclined angle of the contacting object, and both results are plotted at intervals of 5.0 deg. The elastic force increases as the orientation angle increases under constant maximum displacement. As confirmation, we plotted the elastic force against θ_p of Eq. (2.11) in Figure 2.11. The numerical values shown in the graph denote the maximum displacement d . At about 0 deg, there is a clear local minimum of the elastic force, and the change in elastic force with θ_p is greatest when the displacement is maximum, that is, 8.0 mm. The same tendency can also be seen in the simulation results. The results therefore indicate that our proposed elastic model can present a distinctive phenomenon, i.e., a local minimum elastic force, even when the deriving process is represented simply by bringing linear virtual springs standing in the normal direction. On the other hand, the discrepancy in the large displacement shown in Figure 2.11 would be reduced if the Young's modulus could be defined as a nonlinear function of compression strain, and be used to adopt the model to accommodate the nonlinearity of the material. However, the present study focuses on the geometric nonlinearity, and the deriving process including both nonlinearities will be addressed in Chapter 3.

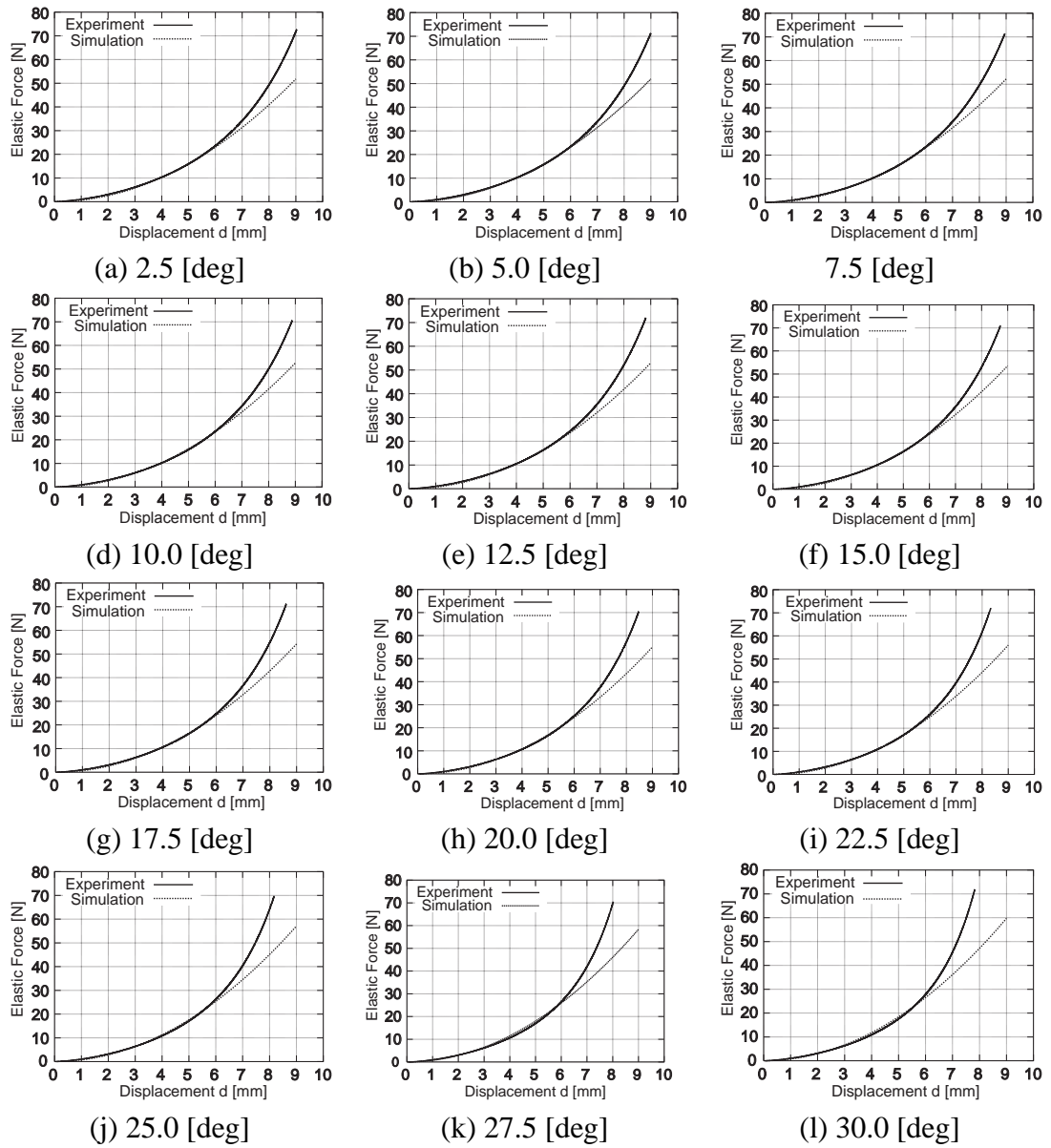


Figure 2.8: Elastic forces in experiments.

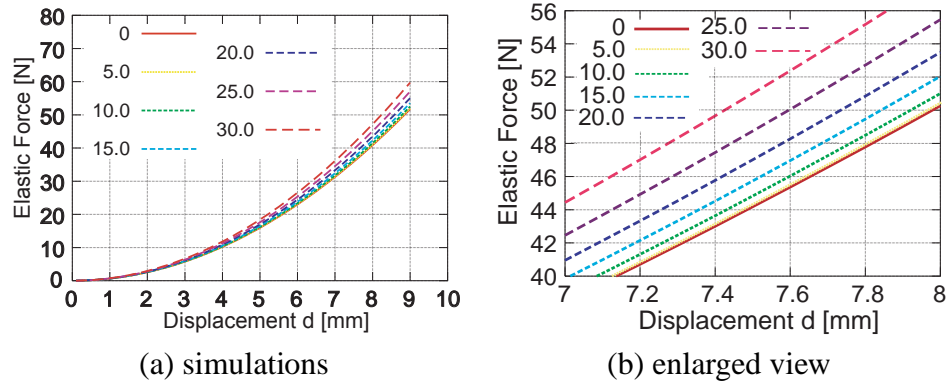


Figure 2.9: Simulation results of elastic force.

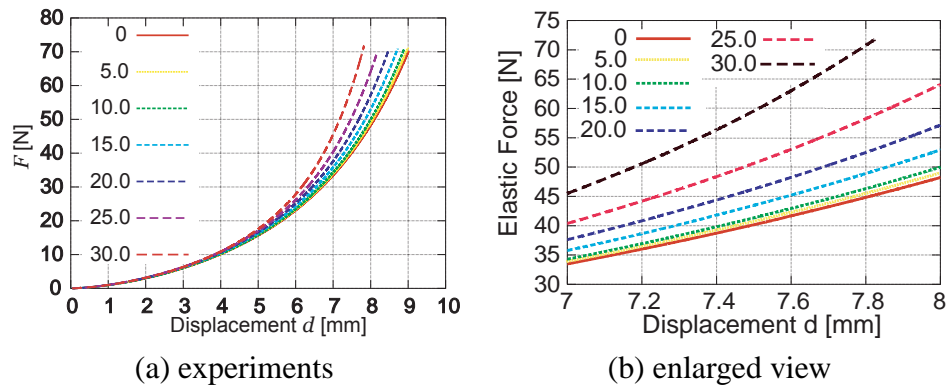


Figure 2.10: Experimental results of elastic force.

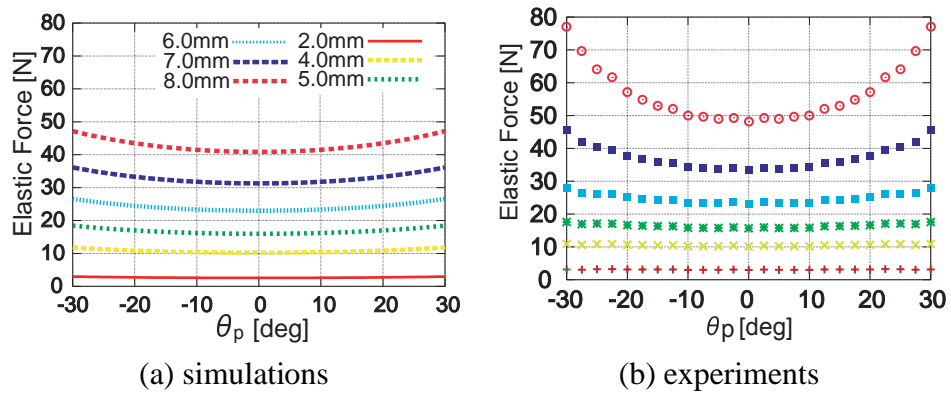


Figure 2.11: Local minimum of elastic force.

2.6 Concluding Remarks

We have formulated a static elastic force model and an elastic potential energy function based on virtual springs inside a hemispherical soft fingertip. We have also proven the existence of an LMEE and experimentally demonstrated that the elastic force due to the deformation has a local minimum. Our model requires us to only measure the Young's modulus of a corresponding material to be used in robotic fingertips. In future studies, we will consider constant volume deformation of incompressible elastomer materials.

These new findings are able to suggest a quasi-static manipulation theory based on the LMEE for a minimum d.o.f. robotic hand [20,21]. By expanding the new idea of LMEE in the development of grasping and manipulation theory using soft-fingered robotic hand, it is expected that the stable grasping and the pose control of a grasped object by a minimum d.o.f. two-fingered hand may be achieved and a succinct control system will be designed.

Chapter 3

Geometrical and Material Nonlinear Elastic Model

The elastic force and elastic potential energy equations derived in Chapter 2 enable us to perform an analytical observation of the control design and the stability problem in soft-fingered handling. Meanwhile, there exists an application field that needs an approach of numerical analysis, but not the analytical approach. For example, the numerical analysis field includes a contact deformation model between multiple soft objects and its elastic force formulation in virtual space [22, 23]. If the numerical analysis is applied, it is not necessary to analytically solve the elliptical area integration expressed as Eqs. (2.3), (2.8), and (2.12). That is, we are able to deal with the integrand of these equations as more complicated forms. In other words, the numerical analysis allows us to incorporate the material property of soft objects such as rubber materials. By applying the material nonlinearity that is obvious in elastomer materials, we extend the elastic force formula, Eq. (2.8), previously discussed in Chapter 2 to a more adequate model closer to real fingertip deformation.

In this Chapter, we clarify the stress-strain relationship of polyurethane gel used as a hemispherical soft fingertip, and then obtain an approximated nonlinear Young's modulus. By substituting the nonlinear Young's modulus into Eq. (2.8), we formulate the more accurate force model by means of the numerical analysis.

3.1 Hertzian Contact and Kao's Elastic Model

In 1881, Hertz proposed a contact theory for two elastic objects having arbitrary curved surfaces [24]. He showed that a normal contact force generated between an elastic sphere and a plane whose Young's modulus is infinity can be expressed as:

$$F = \frac{4\sqrt{R}}{3} \left(\frac{E}{1-\sigma^2} \right) d^{\frac{3}{2}}, \quad (3.1)$$

where R is the radius, E the Young's modulus of the object, σ the Poisson's ratio, and d the maximum displacement of the sphere. Since the above equation is useful from a practical viewpoint, it has been widely used for computing the contact stress between, for example, a wheel and a rail, a roll and material, and a retainer and a ball in a bearing. However, in Hertzian contact, it is assumed that both elastic objects are open elliptic paraboloids with an arbitrary radius of curvature. Consequently, no boundary conditions are used in the Hertzian contact model.

Kao *et al.* defined the parameter c_d corresponding to a material and geometric nonlinearity [11], and transformed Eq.(3.1) into

$$F = c_d d^\zeta. \quad (3.2)$$

They conducted a vertical compression test using a hemispherical soft fingertip, and estimated the parameter c_d empirically by using a weighted least-squares method. It has been shown that ζ is approximately 2.3 or 1.75 when the rate of deformation of the finger is above or below 20%, respectively. In other words, the parameter ζ is not identical to 3/2 in the contact model of soft fingertips. Thus the Hertzian contact theory cannot be adopted for deriving the elastic model of the hemispherical soft fingertip.

3.2 Identification of Nonlinear Young's Modulus

We obtain a nonlinear Young's modulus by compressing several cylindrical soft specimens, which is made of same material with the soft fingertip. Specifically, three cylinders were 20 mm in height and 20, 30, and 40 mm in diameter, and three were 25 mm in height and

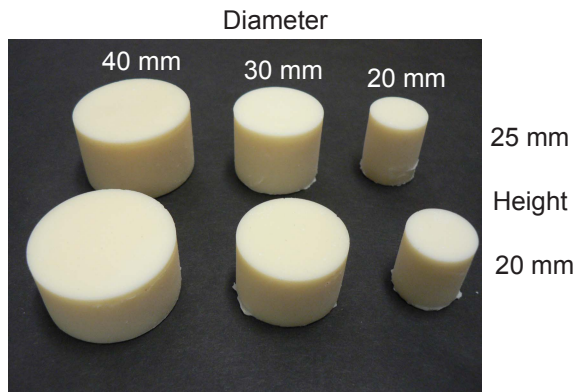


Figure 3.1: Cylindrical specimens

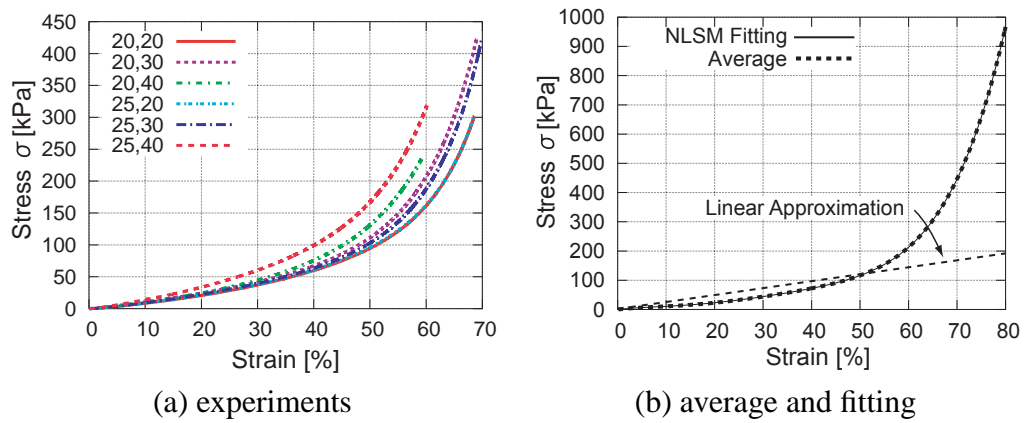


Figure 3.2: Stress strain diagram

also 20, 30, and 40 mm in diameter, as shown in Figure 3.1. Note that we newly made the several specimens for measuring the nonlinear Young's modulus, and these specimens are not same to those exhibited in Figure 2.2-(b).

Figure 3.2-(a) shows the stress-strain diagram of individual specimen, and Figure 3.2-(b) presents a result obtained by performing Nonlinear Least-Square Method (NLSM) to an average value of the diagram, on which a linearly-approximated curve upon 50% compression strain is plotted together with the nonlinearly fitted curve. We apply the linear Young's modulus, $E = 0.232$ MPa, to Eqs. (2.11) and (3.1), in which the modulus corresponds to the slope of linearly-approximated curve depicted in Figure 3.2-(b).

On the other hand, performing a quintic nonlinear approximation (see Appendix E) of the stress with respect to the strain as shown in Figure 3.2-(b), we obtain a following result:

$$\begin{aligned}\sigma(\varepsilon) &\cong 1.829\varepsilon - 1.455 \times 10^{-1}\varepsilon^2 + 8.778 \times 10^{-3}\varepsilon^3 \\ &- 1.908 \times 10^{-4}\varepsilon^4 + 1.548 \times 10^{-6}\varepsilon^5.\end{aligned}\quad (3.3)$$

Defining the nonlinear Young's modulus as the slope of the nonlinear stress-strain diagram, the Young's modulus can then be calculated by differentiating Eq. (3.3) with respect to the strain ε as

$$\begin{aligned}E(\varepsilon) &\cong 1.829 - 2.910 \times 10^{-1}\varepsilon + 2.633 \times 10^{-2}\varepsilon^2 \\ &- 7.632 \times 10^{-4}\varepsilon^3 + 7.740 \times 10^{-6}\varepsilon^4.\end{aligned}\quad (3.4)$$

Substituting the above equation into Eq. (2.8), we obtain an elastic force formula including the material nonlinearity together with the geometrical nonlinearity of the hemispherical soft fingertip:

$$F = \int_{ell} E(\varepsilon) \cdot \varepsilon dS, \quad (3.5)$$

where ε is expressed in Eqs. (2.1) and (2.2) as

$$\varepsilon = 1 - \frac{a - d - x \sin \theta_p}{\cos \theta_p \sqrt{a^2 - (x^2 + y^2)}}. \quad (3.6)$$

As mentioned above, it is sufficient to use Eq. (3.5) instead of Eq. (2.11) as the elastic force formula when we do not need to analytically solve equations of motion of a grasped object in soft-fingered manipulation.

3.3 Comparison with Hertzian Contact

Figure 3.3 shows a comparison result in which the elastic force value with respect to the displacement d is plotted when a hemispherical soft fingertip is compressed vertically, whose radius is 20 mm, as shown in Figure 2.2-(a). Here, the reason for choosing a vertical contact between the object and the fingertip is that the Hertzian contact does not have the contact orientation, θ_p . Since it is impossible to compare Eqs. (2.11) and (3.5) with the Hertzian contact theory expressed as Eq. (3.1) when θ_p has a certain value, we substitute $\theta_p = 0$ into Eqs. (2.11) and (3.5). Finally, we obtained a good adjusted result relative to the material linear elastic model expressed as Eq. (2.11). It is obvious that the vertically-oriented spring model is more suitable for deriving an elastic force through all the deformation range. It is because that our model contains the geometrical nonlinearity due to the hemispherical shape and the material nonlinearity of the fingertip. We can also find that the Hertzian contact theory can not be applied to formulating elastic forces on the soft contact.

Soft materials exhibit nonlinear characteristics, even for infinitesimal deformations. In fact, Tatara newly derived a nonlinear Young's modulus with respect to compressive strain [25]. Furthermore, the concept for the contact angle of the object is not incorporated in the Hertzian contact theory. While the Hertzian contact theory can be utilized for a simple contact pattern corresponding to the normal contact, no contact at any other arbitrary angle or rolling contact can be defined. On the other hand the elastic models proposed in this paper cover any contact angle of the object, and therefore, these models can be used to analyze grasping and manipulating motions containing varied possible contact forms by soft-fingered robotic hand.

Note that we experimentally measured the elastic forces on a soft fingertip by means of a load cell with a compression machine produced by INSTRON Co., LTD.. In addition, we used $E = 0.232$ MPa to measure the elastic forces.

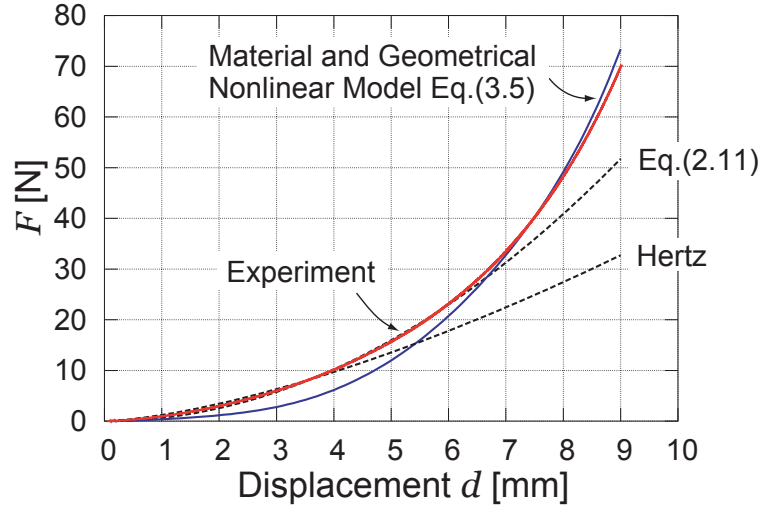


Figure 3.3: Comparison between the material nonlinear elastic force model and conventional force models (Eq. (2.11) and Hertzian model) when $\theta_p = 0$ and $E = 0.232$ [MPa].

3.4 Force Comparison

In this section, we compare the geometrical and material nonlinear elastic force expressed as Eq. (3.5) with Eq. (2.11) when the orientation angle θ_p becomes 2.5 deg to 30.0 deg at the interval of 2.5 deg.

As shown in Figure 3.4, we obtained preferable results even in the large deformation range in spite of the change of the object orientation. However, while the experimental data becomes large than the theoretical data in the small deformation range, the theoretical data becomes relatively large than the experimental data in the large deformation range. This phenomenon comes from an intrinsic elastomer characteristics corresponding to a physical property that the rate of increase of the fingertip stiffness is different between large deformation and small deformation [11]. Additionally, the theoretical data shifts toward left side on the Figures according to the increase of object orientation angle θ_p . In order to clarify the phenomenon, we show comparison results of experiment and simulation respectively, as depicted in Figure 3.5. In the Figure, the result of each elastic force curve is shown when θ_p changes from 0 deg to 30 deg at the interval of 5 deg.

In simulation results on Figure 3.5-(a), the rate of change of the force through the

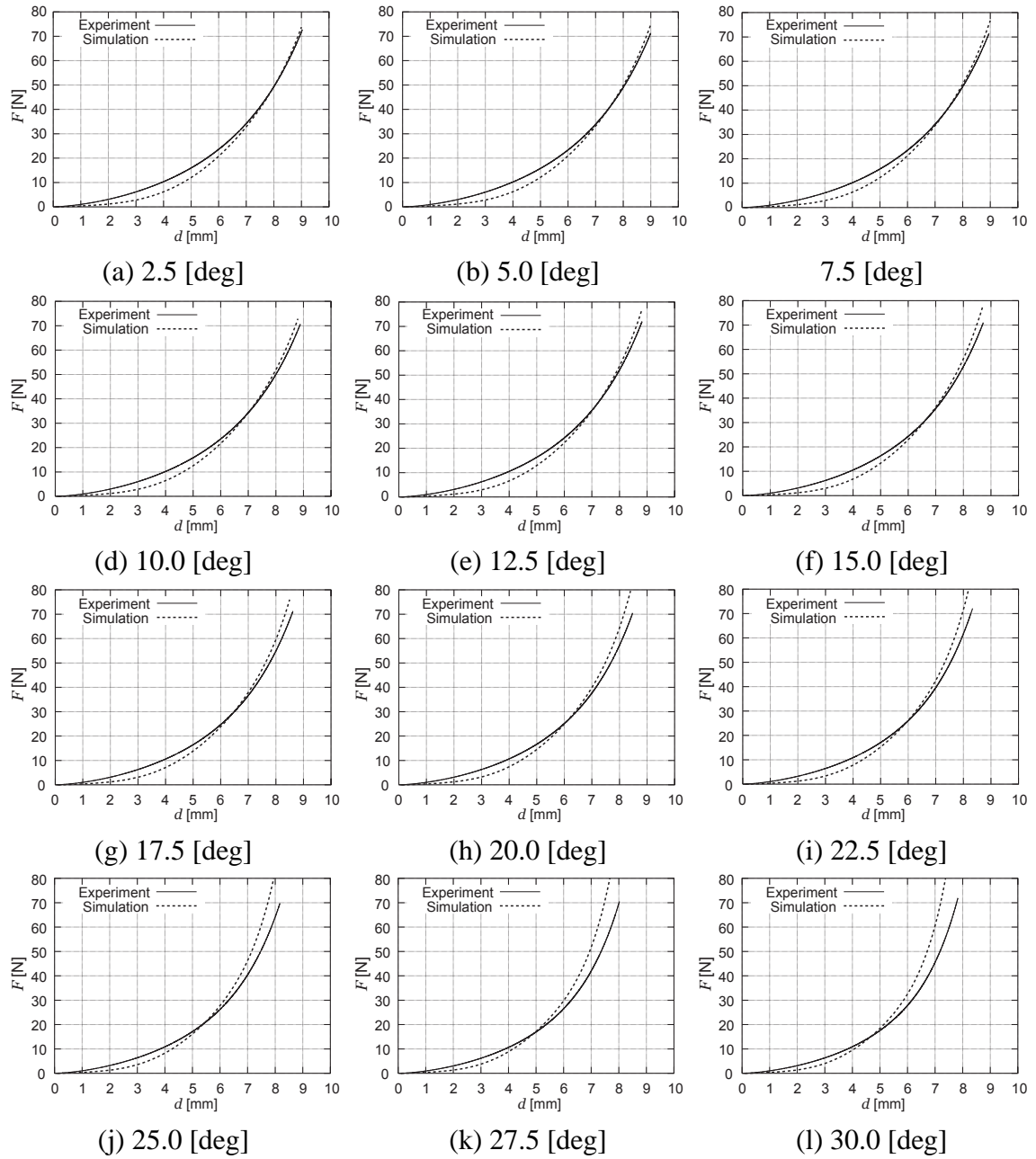


Figure 3.4: Comparison between elastic forces in geometrical and material nonlinear model.

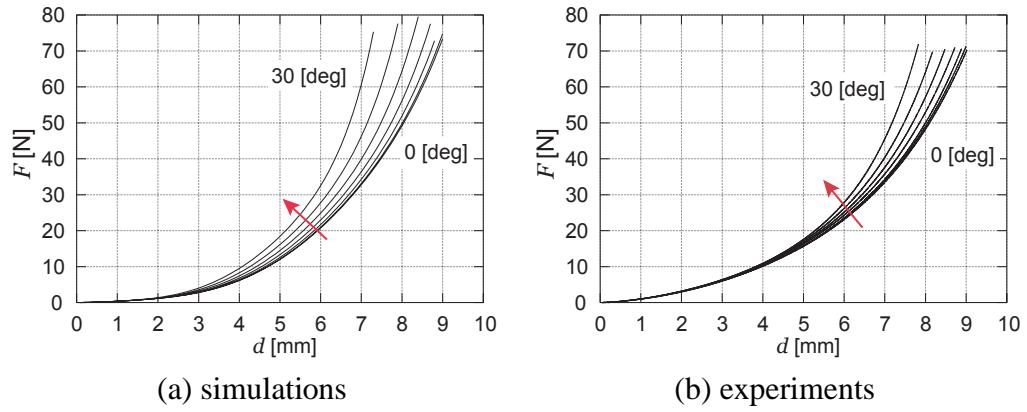


Figure 3.5: Comparison between simulations and experiments

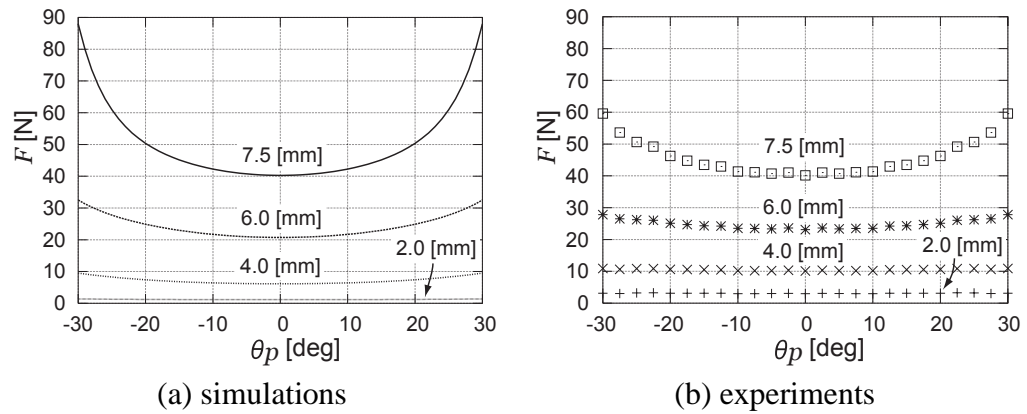


Figure 3.6: Local minimum of elastic forces

increase of contacting angle, and such trend can be seen especially in the small deformation area. On the other hand, in the case of experimental results shown in Figure 3.5-(b), the slope of the force changes little up to approximately $d=5$ mm.

In addition, as shown in Figure 3.6 a local minimum point of the elastic force appears when the normal contact force with several orientation angle applied to the soft fingertip. During the large orientation angle, we can find a large discrepancy especially on ± 30 deg. This result comes from the fact that while the fingertip easily deforms along lateral direction in actual compression, such complicated motion of the fingertip never happen in simulation. Therefore, the force applied to the fingertip is directly transmitted to the bottom surface in simulation, and it increases the force result in Figure 3.6-(a).

3.5 Concluding Remarks

In this Chapter, we have defined a nonlinear Young's modulus of soft fingertip, which is directly computed from a stress-strain data measured by a compression test. By using the nonlinear Young's modulus, we have successfully modified the force-displacement diagram depicted in Figure 2.8.

Chapter 4

Quasi-Static Manipulation with Soft Fingers

Up to the previous Chapters, we have focused on the elastic force and potential energy associated with large deformation of a hemispherical soft fingertip, and showed that the elastic potential energy has a local minimum that is abbreviated to LMEE: "*Local Minimum of Elastic Potential Energy*". We derived two equations, one for the elastic force and one for the potential energy. Both equations are functions of the displacement of the fingertip and the posture of contact between the fingertips and the object.

In this Chapter, we propose a new quasi-static manipulation methodology based on the LMEE numerical algorithm using two-fingered robotic hand with minimum degrees of freedom [20]. We demonstrate that the quasi-static manipulation theory can determine unique position and orientation of the manipulated object by the soft-fingered hand.

4.1 Geometric Constraints

Below, we formulate two sets of geometric constraints, normal and tangential, for a soft-fingered robotic hand with two rotational joints grasping and manipulating a planar rigid object, as illustrated in Figure 4.1.

4.1.1 Normal Constraints

Consider the manipulation process of a soft-fingered, minimum d.o.f. robotic hand two-dimensionally, ignoring gravitation, as illustrated in Fig.4.1. We formulate two geometric constraints along the normal direction to both sides of a planar object grasped by the two-fingered hand.

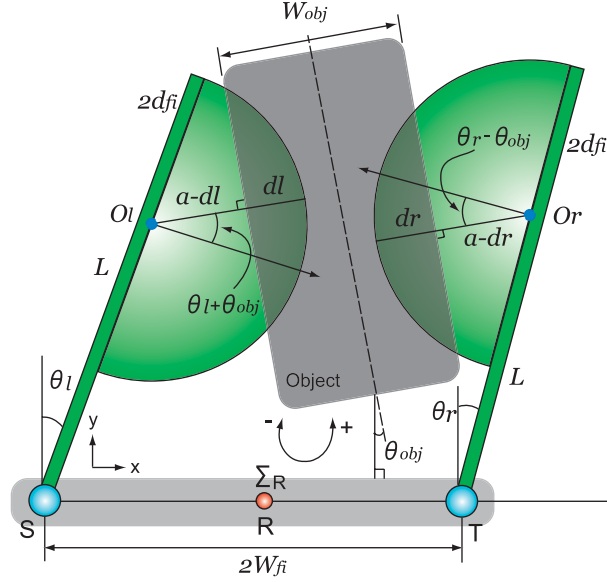


Figure 4.1: Soft-fingered manipulation

Let a be the radius, (d_r, d_l) be the right and left maximum displacements of the soft fingertip, L be the length of the finger, and W_{obj} be the width of the grasped object. Let $2W_{fi}$ be the width of the fingers at their base, and $2d_{fi}$ be the thickness of the finger. Furthermore, let (θ_r, θ_l) be a pair of rotational angles of both fingers, (O_r, O_l) be the fingertip origin, and R be the origin of the reference coordinate system Σ_R with respect to the midpoint of $2W_{fi}$. Letting θ_{obj} be the orientation angle of the object with respect to Σ_R , which is positive counter-clockwise, coordinates of points (O_r, O_l) are described with respect to Σ_R as follows:

$$\mathbf{O}_r = \begin{bmatrix} W_{fi} - L \sin \theta_r - d_{fi} \cos \theta_r \\ L \cos \theta_r - d_{fi} \sin \theta_r \end{bmatrix}, \quad (4.1)$$

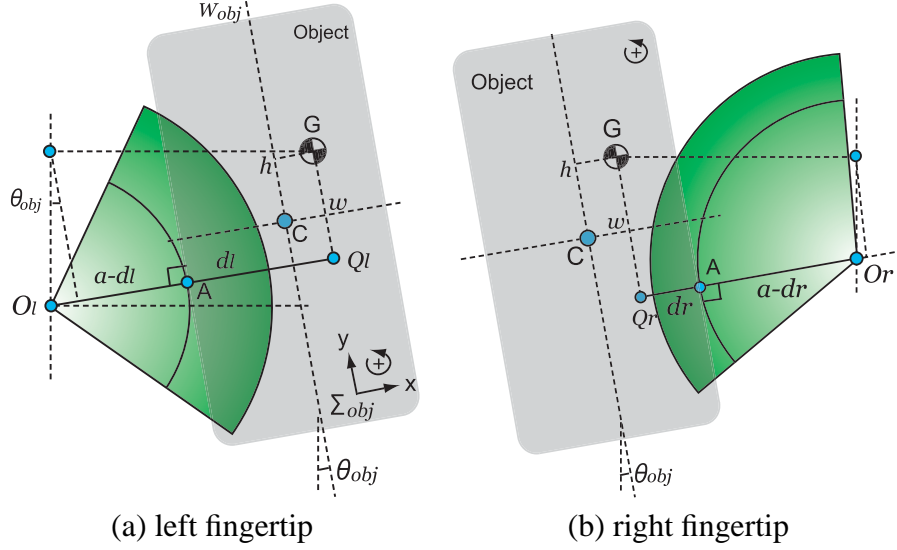


Figure 4.2: Normal constraints

$$\mathbf{O}_l = \begin{bmatrix} -W_{fi} + L \sin \theta_l + d_{fi} \cos \theta_l \\ L \cos \theta_l - d_{fi} \sin \theta_l \end{bmatrix}. \quad (4.2)$$

As shown in Figure 4.2-(a) for the left fingertip, let Σ_{obj} be the object coordinate system that has the origin C , and $G(x_{obj}, y_{obj})$ be the center of gravity of the grasped object with respect to Σ_R , which equals to (w, h) in Σ_{obj} . Letting A be the center of contacting circular area, and Q_l be the foot of a perpendicular dropped on the line O_lA , the length of O_lQ_l can be represented as follows:

$$O_lQ_l = (x_{obj} - O_{lx}) \cos \theta_{obj} + (y_{obj} - O_{ly}) \sin \theta_{obj}. \quad (4.3)$$

We derive a geometric constraint when plane-contact occurs with the maximum displacement d_l .

$$\begin{aligned} (x_{obj} - O_{lx}) \cos \theta_{obj} + (y_{obj} - O_{ly}) \sin \theta_{obj} \\ = (a - d_l) + \frac{W_{obj}}{2} + w. \end{aligned} \quad (4.4)$$

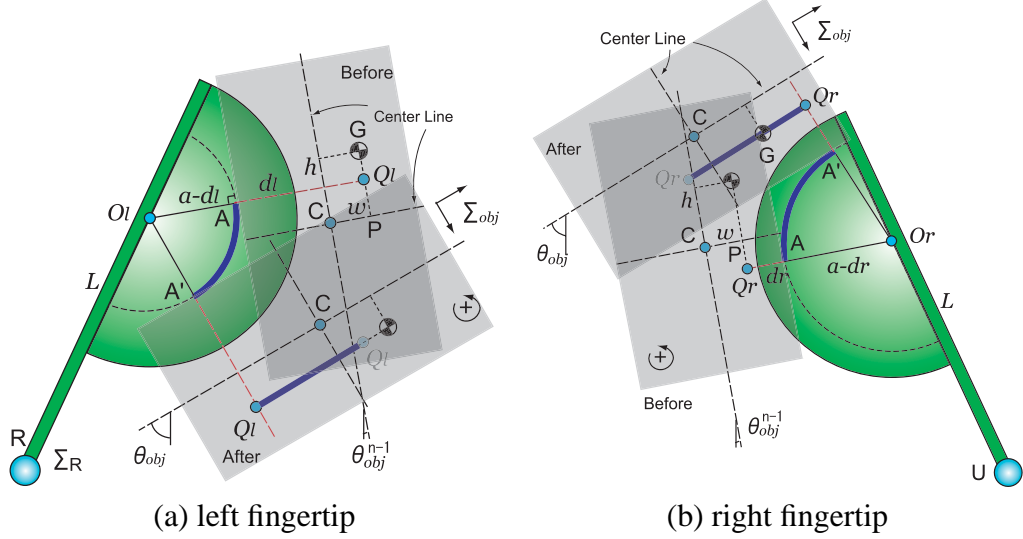


Figure 4.3: Tangential constraints

We obtain another equation for the right fingertip shown in Figure 4.2-(b).

$$\begin{aligned}
 & -(x_{obj} - O_{rx}) \cos \theta_{obj} - (y_{obj} - O_{ry}) \sin \theta_{obj} \\
 & = (a - d_r) + \frac{W_{obj}}{2} - w,
 \end{aligned} \tag{4.5}$$

where (O_{rx}, O_{ry}) and (O_{lx}, O_{ly}) denote xy -coordinates in Eqs. (4.1) and (4.2).

Note that the geometric normal constraints for rigid-fingered manipulation can be represented by substituting $(d_r, d_l) = (0, 0)$ into Eqs. (4.4) and (4.5).

4.1.2 Tangential Constraints

To formulate tangential constraints appearing on both fingertips during rolling motion, i.e., *rolling constraints*, we assume that there is no slip between the fingertips and the grasped object.

Let θ_{obj}^k be the k -th object orientation when the object iterates the n -times rolling motion on the fingertip, and for convenience let us use θ_{obj} instead of θ_{obj}^n in what follows. As shown in Figure 4.3-(a) for the left fingertip, draw a straight line through points O_l and A , and let consider the manipulation process of a soft-fingered, minimum d.o.f. robotic hand

two-dimensionally, ignoring gravitation, as illustrated in Figure 4.1. We formulate two geometric constraints along the normal direction to both sides of a planar object grasped by the two-fingered hand. P be the point where the perpendicular line from the center of gravity G intercepts the center line beyond point C . Let Q_l be the intersection with the line O_lA on the above perpendicular, and each point is defined as $P(w, 0)$ and $Q_l(w, s_l)$ using the coordinate system Σ_{obj} . Here, s_l is a position relative in the tangential direction between the point C and the line O_lA . That is, s_l corresponds to a physical quantity and can be the distance that the object has rolled. Consequently, when the object rolls on the soft fingertip with radius $a - d_l$, the length GQ_l is updated by adding the rolling distance AA' as follows:

$$GQ_l = h - s_l - (a - d_l) \cdot (\theta_{obj} - \theta_{obj}^{n-1}), \quad (4.6)$$

where counter-clockwise rolling θ_{obj} is positive. At the same time, a geometric relationship along the tangential direction shown in Figure 4.2-(a) can be described as follows:

$$GQ_l = -(x_{obj} - O_{lx}) \sin \theta_{obj} + (y_{obj} - O_{ly}) \cos \theta_{obj}. \quad (4.7)$$

From Eqs. (4.6) and (4.7), the tangential constraint on the left fingertip can be finally expressed as follows:

$$\begin{aligned} & -(x_{obj} - O_{lx}) \sin \theta_{obj} + (y_{obj} - O_{ly}) \cos \theta_{obj} \\ & = h - s_l - (a - d_l) \cdot (\theta_{obj} - \theta_{obj}^{n-1}). \end{aligned} \quad (4.8)$$

Similarly, the tangential constraint of the object on the right fingertip is

$$\begin{aligned} & -(x_{obj} - O_{rx}) \sin \theta_{obj} + (y_{obj} - O_{ry}) \cos \theta_{obj} \\ & = h - s_r + (a - d_r) \cdot (\theta_{obj} - \theta_{obj}^{n-1}). \end{aligned} \quad (4.9)$$

Note that Eqs. (4.8) and (4.9) are geometric tangential constraints due to the object rolling between both fingertips.

Here, (s_r, s_l) correspond to the sum of the distance of $(n-1)$ active rolls of the object

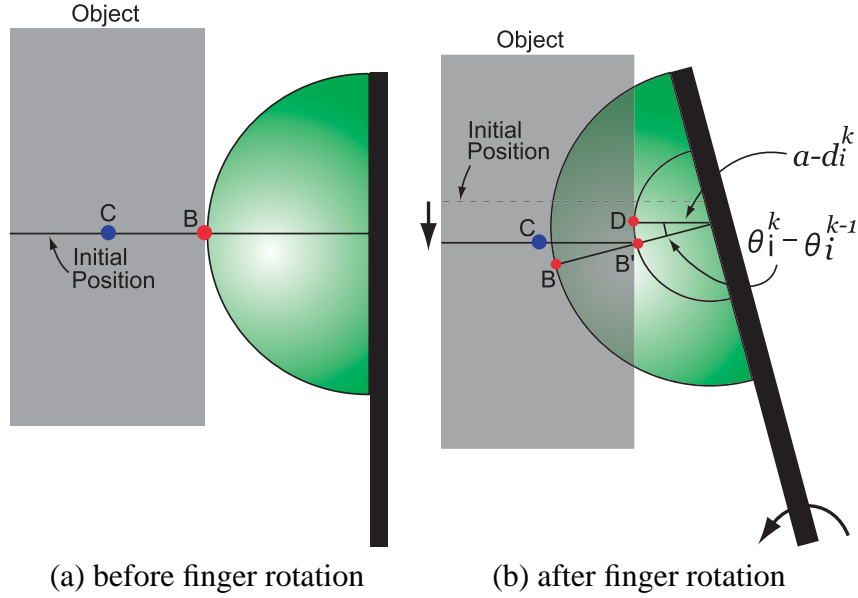


Figure 4.4: Passive rolling

as shown in Figure 4.3 and n passive rolls due to the finger rotation as shown in Figure 4.4,

$$s_i = (-1)^i \sum_{k=1}^{n-1} (AA')_i^k + \sum_{k=1}^n (a - d_i^k) \cdot (\theta_i^k - \theta_i^{k-1}) + s_i^0, \quad (4.10)$$

where

$$(AA')_i^k = (a - d_i^k) \cdot (\theta_{obj}^k - \theta_{obj}^{k-1}),$$

and the symbol i takes 1 or 2 respectively, for the right and left fingertips. Furthermore, θ_i^k denotes the k -th rotational angle of the i -th finger, d_i^k means the k -th maximum displacement of the i -th fingertip, and s_i^0 corresponds to the initial value of s_i . Eq. (4.10) indicates that the first term is equivalent to the sum of the direct rolling distance on the soft fingertip, as shown in Figure 4.3, and the second term corresponds to the sum of DB' of the relative rolling distance along the contacting surface without slip as the finger rotates, as illustrated in Figure 4.4.

4.2 Quasi-Static Manipulation

Now, we define a single handling process with minimum basic motion including rolling and translation by infinitesimal movements of the object while being grasped by both fingertips. In this paper, we consider a quasi-static handling motion by ignoring the dynamics of the finger, the fingertip and the grasped object. Applying the concept of LMEE for large deformation of a soft fingertip, we propose a quasi-static manipulation methodology, in which physical variables $(x_{obj}, y_{obj}, \theta_{obj})$ are determined uniquely through the minimum basic motion.

4.2.1 Algorithm Using Extended LMEE

The concept of LMEE, represented in Eq. (2.14), can be extended for a minimum d.o.f. robotic hand with two rotational joints as follows. As shown in Figure 4.1, the total elastic potential energy due to the deformation of both fingertips is

$$P = \frac{\pi E}{3} \left\{ \frac{d_r^3}{\cos^2(\theta_r - \theta_{obj})} + \frac{d_l^3}{\cos^2(\theta_l + \theta_{obj})} \right\}. \quad (4.11)$$

There are nine variables: $(x_{obj}, y_{obj}, \theta_{obj})$, (θ_r, θ_l) , (d_r, d_l) , and (s_r, s_l) with four constraints given in Eqs. (4.4), (4.5), (4.8), and (4.9). Variables (d_r, d_l) and (s_r, s_l) are described by $(x_{obj}, y_{obj}, \theta_{obj})$ and (θ_r, θ_l) , using normal constraints Eqs. (4.4) and (4.5) and tangential constraints Eqs. (4.8) and (4.9), respectively. Assuming that the finger joint angles (θ_r, θ_l) are input variables, the procedure of the quasi-static manipulation process can be summarized as follows:

1. Each finger joint angle (θ_r, θ_l) is arbitrarily given as an input angle.
2. An LMEE is computed from Eq. (4.11).
3. $(x_{obj}, y_{obj}, \theta_{obj})$ are all determined from the LMEE value.
4. (d_r, d_l) and (s_r, s_l) are calculated from the above $(x_{obj}, y_{obj}, \theta_{obj})$.

Here, we assume that the grasped object is a rigid rectangular solid. We also assume that slip between the object and the soft fingertip is negligible, and all manipulation and grasping processes are confined to a two-dimensional plane without the effect of gravity.

4.2.2 Method of Numerical Analysis

We explain a more general method of the LMEE algorithm, which is based on the analytical approach. In this soft-fingered manipulation system illustrated in Figure 4.1, we consider independent variables as $\mathbf{p} = [x_{obj}, y_{obj}, \theta_{obj}, \theta_r, \theta_l]^T$. On the other hand, each rolling distance on a soft fingertip differs when the sequence of the rolling and translational motions within the minimum basic motion is reversed. This fact results in a discrepancy for the position of point C in terms of the y -coordinate distance with respect to Σ_{obj} . In other words, these tangential constraints have a dependence on the history of the basic motion. In order to avoid the growing complexity of this, we assume that the infinitesimal rolling motion occurs after the infinitesimal translational motion.

The internal energy function I for both fingertip deformations can be defined as:

$$I(\mathbf{p}, \mathbf{f}) \triangleq P - \mathbf{f}^T \cdot \mathbf{g}, \quad (4.12)$$

where $\mathbf{f} = [f_1, f_2, f_3, f_4]^T$ denotes an undetermined constant set, and \mathbf{g} corresponds to the normal and tangential constraint vectors described in Eqs. (4.4), (4.5), (4.8), and (4.9). A set of the independent variables is computed such that the internal energy function satisfies the LMEE. Thus, the more general expression of the quasi-static manipulation theory based on the LMEE algorithm can be expressed as follows:

$$\begin{aligned} &\text{Minimize } I \\ &\text{Subject to } \mathbf{g} = \mathbf{0}. \end{aligned} \quad (4.13)$$

Since each rotational angle of each finger is an input angle and hence a known value, the manipulation system has three independent variables:

$$\mathbf{p} = [x_{obj}, y_{obj}, \theta_{obj}]^T. \quad (4.14)$$

Consequently, the static equilibrium conditions of the proposed manipulation system can be described as seven nonlinear simultaneous equations as follows:

$$\frac{\partial I(\mathbf{q})}{\partial \mathbf{q}} = \mathbf{0}, \quad (4.15)$$

where $\mathbf{q} = [x_{obj}, y_{obj}, \theta_{obj}, f_1, f_2, f_3, f_4]^T$. By computing Eq. (4.15) in a numerical analysis, we confirm that the three variables above converge to an LMEE point.

4.3 Simulation

In the first step described in the above section, each joint angle of each finger moves while remaining in contact with the grasped object. In the the second step, in search of the LMEE point for each infinitesimal change in joint angle, the *Nelder-Mead Method* is applied to Eq. (4.13), in which I and $\mathbf{g} = \mathbf{0}$ are respectively defined as a target function and constraint equations in the numerical computation. In the fourth step, each maximum displacement of each fingertip is calculated by substituting, into Eqs. (4.4) and (4.5), $(x_{obj}, y_{obj}, \theta_{obj})$ computed in the third step.

The handling process in the simulation can be summarized as follows:

1. As shown in Figure 4.5-(a) and (b), both fingers rotate by a certain degree to the inner side from an initial condition ($\theta_r = \theta_l = d_r = d_l = 0$) (operation 1). In this paper, we simulate manipulation tasks associated with five different grasping angles, where (θ_r, θ_l) simultaneously increases from 2.4 deg to 7.2 deg in increments of 1.2 deg.
2. Both fingers rotate counter-clockwise by 20 deg as shown in Figure 4.5-(c) (operation 2).
3. Both fingers rotate toward clockwise by 40 deg as shown in Figure 4.5-(d) (operation 3).
4. Both fingers rotate counter-clockwise direction by 40 deg.
5. Steps 3 and 4 iterate three times.

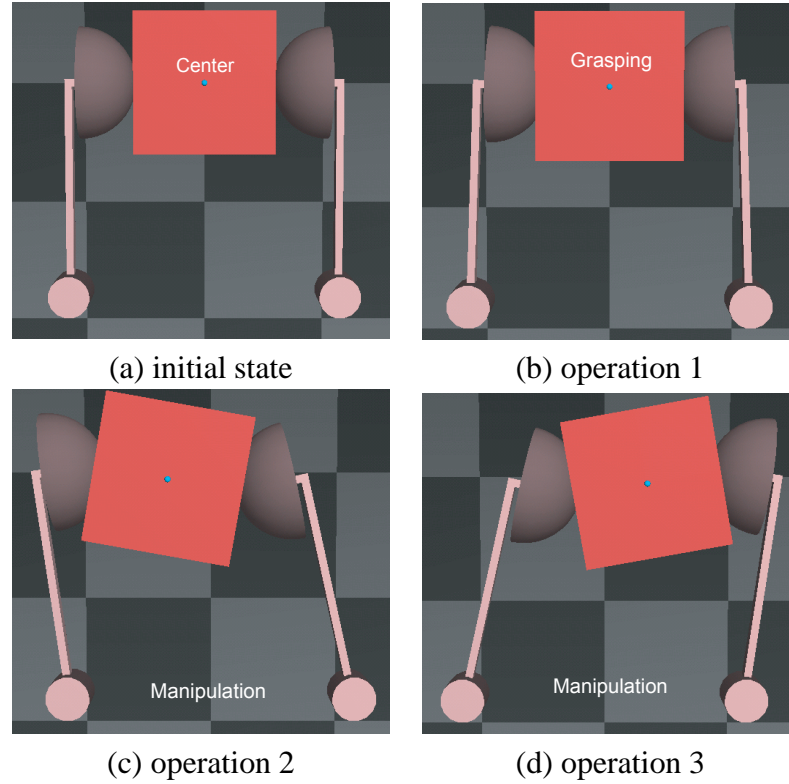


Figure 4.5: Quasi-static manipulation process

6. Both fingers go back to the condition of operation 1.
7. Both fingers go back to the initial condition.

All the parameters used in this simulation were set equal to those of the double-jointed robotic hand made for the physical experiment. For simplicity, we also set that the center of gravity of the object G and the geometric center C as identical to each other. That is, the coordinate of $G(w, h)$ with respect to Σ_{obj} is $(0, 0)$, as shown in Figure 4.3. All the simulation results are given in the results.

4.4 Experiments

A planar, rigid rectangular object was grasped and manipulated by a minimum d.o.f. soft-fingered robotic hand, with two rotational joints, as shown in Figure 4.6. To validate the

Table 4.1: System parameters

| Parameters | Values |
|-----------------------------|---------------|
| Finger length : L | 76.2 [mm] |
| Fingertip radius : R | 20 [mm] |
| Object width : W_{obj} | 49 [mm] |
| Finger thickness : d_{fi} | 4 [mm] |
| Young's modulus : E | 0.30378 [MPa] |
| Gear ratio | 108 |
| Input pulse | 1 [kHz] |

quasi-static manipulation theory based on the LMEE algorithm, the position and orientation of the object was monitored using a CCD camera and compared with the simulation results. Here, we discuss the feasibility of the fine manipulation with the soft fingertip based on new findings in this experiment.

4.4.1 Apparatus and Parameters

As shown in Figure 4.6, two stepping motors were used to drive two fingers with hemispherical soft tips. The fingertip had a diameter of 40 mm and the grasped object had an area of 49 mm² on the top side in the apparatus. We limited the movements of the object and fingers to two-dimensional plane. All the parameters for the robotic hand are shown in Table 4.1. We applied a Young's modulus measured by the tensile test of the polyurethane rubber from which the fingertips were made.

4.4.2 Experimental Method

A rectangular sheet of black paper was attached to the object. The object's center of gravity was taken to coincide with the luminance center of a binary image (Figure 4.7) of the paper, obtained using a CCD camera above the robotic hand. The object orientation angle was measured by computing the second order moment of the binary image.

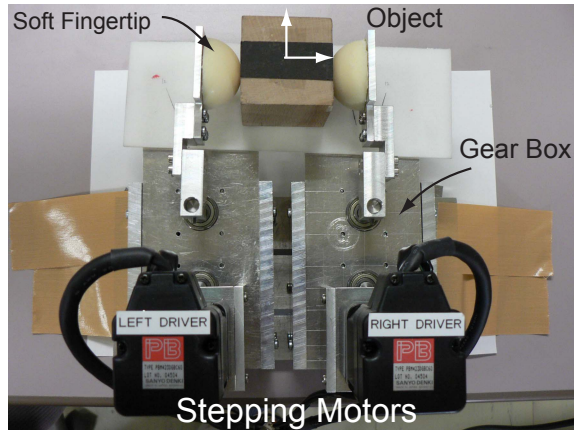


Figure 4.6: Apparatus

4.4.3 Experimental Results

Figure 4.8 is a plot of simulated and experimental results. The left column shows the path of the center of gravity (x_{obj}, y_{obj}) during the grasping and manipulation processes, while the right column shows the change in the orientation of the object.

The grasping angle is 2.4 deg at operation 1 in the top graphs, and increases by 1.2 deg per row, becoming 7.2 deg in the bottom graphs. The origin of each graph corresponds to the center of the paper on the object, as shown in Figure 4.6.

In the grasping motion, the position of the object, shown in the left column, totally shifts downwards much. In the manipulating motion, we find that both resultant curves are close to each other as well as the grasping motion. Furthermore, the experimental curve deviates downward relative to the simulation curve as the grasping angle becomes large. This results from the soft fingertip deforming much laterally as the grasping angle gets larger. Thus, the grasped object sinks downward in the experimental set up but not in the simulation.

On the other hand, in the experiments, the orientation results shown in the right column of Figure 4.8 indicate that an S-shaped curve appears explicitly in every graph. This results from the rolling distance on the fingertip increasing as the rolling motion progresses in the manipulation process. Therefore, the rate of change of the object orientation decreases as the object rotation proceeds towards both ends of the S-shaped curve. A slight S-shaped

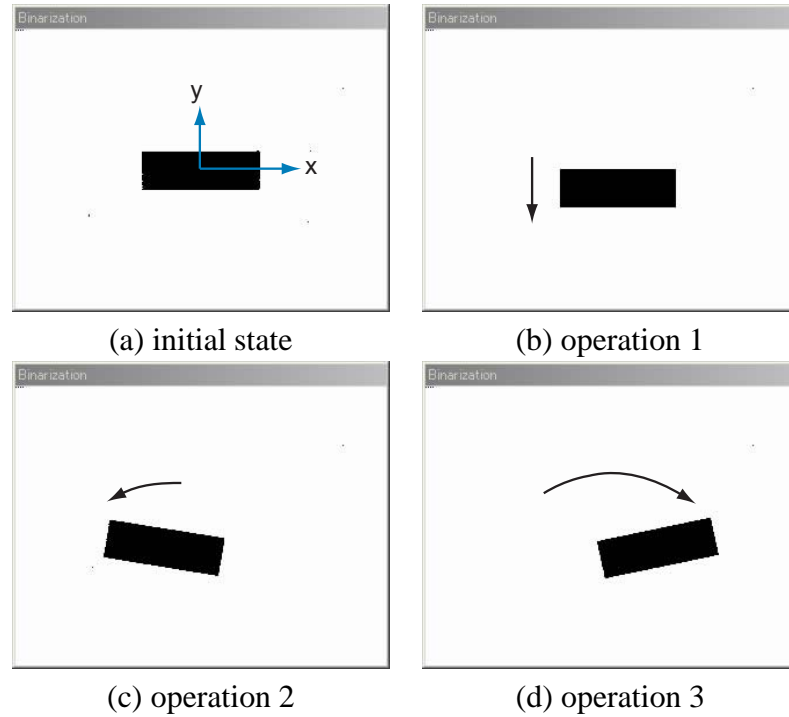
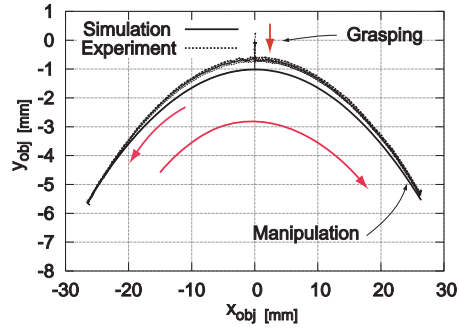


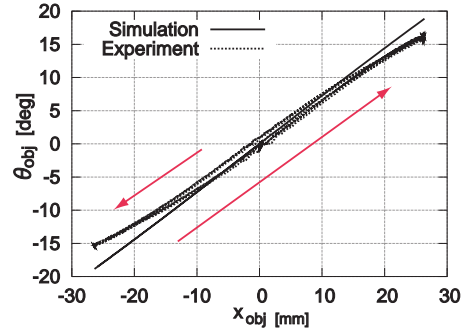
Figure 4.7: Binary images

curve also occurred in the simulation results. Some discrepancies between the simulation and experimental results appear when x_{obj} becomes large, because the experimental rolling radius during the manipulating motion is somewhat larger than that in the model, represented in normal and tangential constraints. Furthermore, a relatively large discrepancy is found in the bottom graph, in which the grasping angle is 7.2 deg. This is attributable to difference in actual and simulated rolling radius, which becomes increasingly large with increasing grasping angle. The difference in the rolling distance on a soft fingertip therefore increases as the object rotation proceeds during the manipulation.

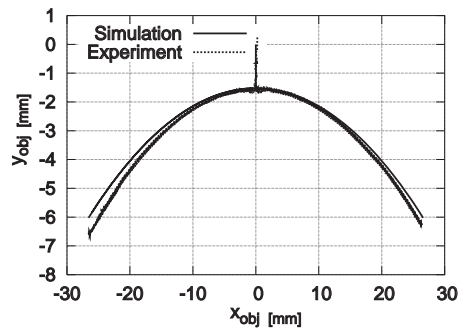
Figure 4.9 is a comparison of the path of the object in all the experimental results. Note that each end point of the path of the manipulation process conforms closely to all together at approximately ± 28 mm although both rotational angles (θ_r, θ_l) after operations 2 and 3 are always different for all five grasping angles. This consistency in x_{obj} implies that the x -coordinate of the object position does not depend on the magnitude of grasping force which is equivalent to the elastic force of the soft fingertip. In other words, in order to transfer



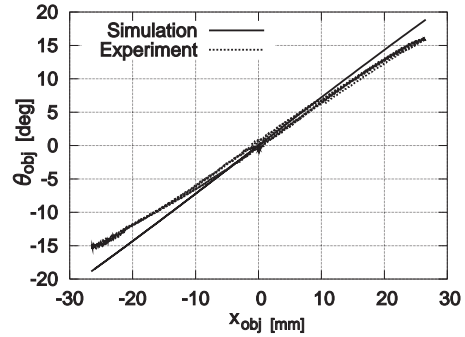
(a) position in 2.4[deg]



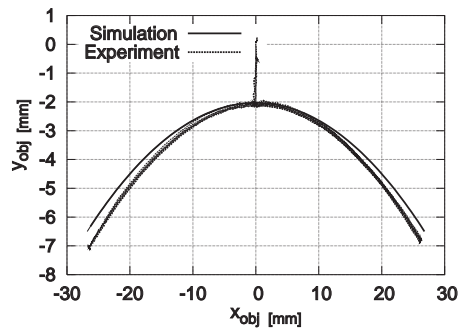
(b) orientation in 2.4[deg]



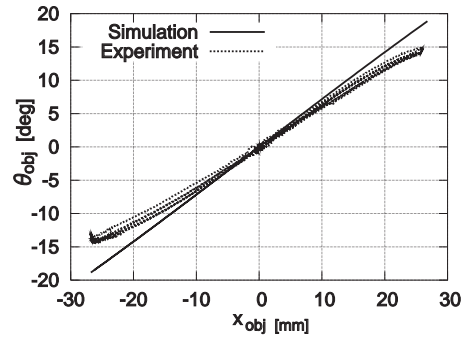
(c) position in 3.6[deg]



(d) orientation in 3.6[deg]



(e) position in 4.8[deg]



(f) orientation in 4.8[deg]

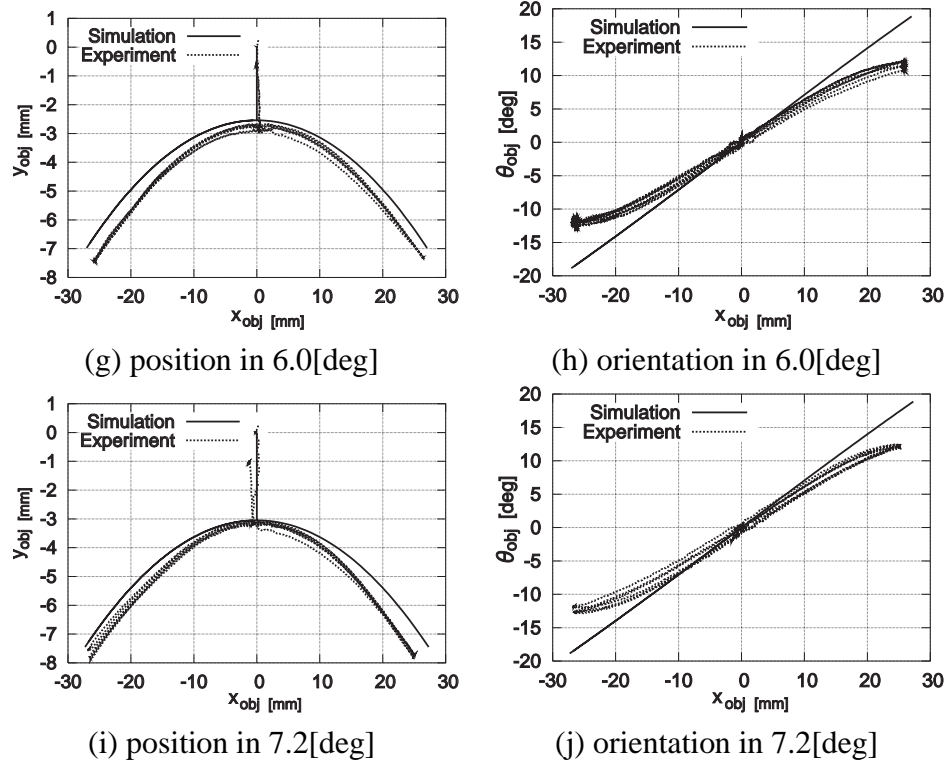


Figure 4.8: Comparison with simulation and experiment

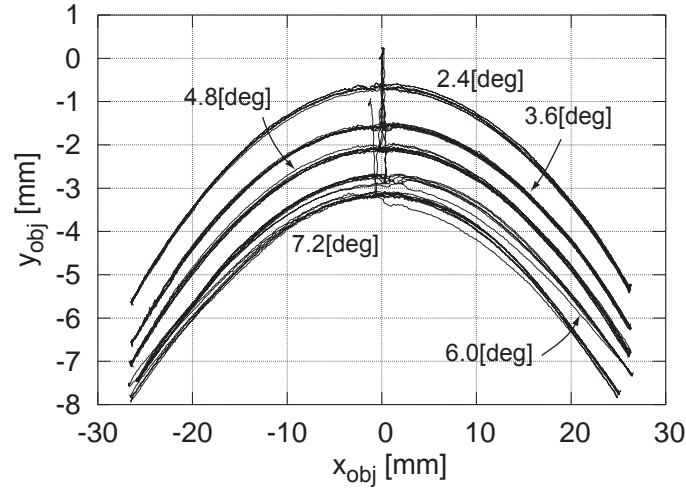


Figure 4.9: Comparison of object position in experiments

an object to a certain position on the x -axis, it is only necessary to activate the fingers by a certain degree that corresponds one-to-one with the position of the object irrespective of the elastic force level of the fingertip. Furthermore, it is obvious that y_{obj} is determined by the elastic force level.

4.5 Concluding Remarks

In this paper, we have proposed a quasi-static manipulation methodology based on the LMEE algorithm, which is described by summing both elastic potential energies due to large deformation of hemispherical soft fingertips mounted on a two-fingered robotic hand. Also, we have shown that the position and the orientation of a grasped object can be uniquely determined in the two-dimensional plane in a numerical analysis, in which two geometric relationships and two tangential constraints during soft-fingered grasping tasks are derived. We have validated the proposed theory by comparing measured positions and orientations of a grasped object with simulation results of the two-fingered manipulation process.

We believe that the discrepancies between the real and simulated results can be reduced by including a constant volume effect for the hemispherical soft fingertip. That is, it is

necessary to incorporate into our elastic model the effect due to the incompressibility of soft materials. This is essential for fine manipulation by soft fingertips, and is an important factor in deriving and analyzing the dynamics of the total handling system based on a viscoelastic model.

The findings relating to the LMEE due to large deformation of the hemispherical soft fingertip enables us to describe a straightforward control law for the dynamic manipulation of a grasped object. Also, we expect that a complicated control system for conventional rigid-fingered handling can be avoided. We will consider the lateral deformation effect of the soft fingertip, and explore the dynamic analysis of total handling system with soft fingertips. Further studies on the above experimental phenomena and the theoretical analysis of dynamic grasping and manipulating motions will be valuable for fine manipulation using soft fingertips.

Chapter 5

Dynamic Manipulation with Soft Fingers

In the case of dealing with soft-fingered manipulation, the modeling of elastic soft materials is much important. While a pretty accurate elastic model is able to describe a true behavior of an object grasped by soft fingers, it is extremely difficult to represent the exact model in an analytical procedure. Generally, nonlinear Finite Element analysis is used for computing the elastic force and showing the deformation process, whose model is based on experimental observations but not analytical ways. Hence, when we discuss the soft-fingered manipulation analytically, it is important how much we can get the model to be closer to an appropriate model that is able to express a real object motion through the soft fingertips.

Furthermore, modeling issue of soft fingers is intimately connected to not only modeling itself, but also stable grasping and robust manipulation in the robotic hand system as well. That is, position/posture controls of the grasped object without complicated control inputs that is usually designed for the conventional point-contact manipulation can be demonstrated by using the more suitable soft fingertip model.

In this paper, we first extend previous one-dimensional fingertip model to two-dimensional model by additionally applying the bending motion of the fingertip along the tangential direction of grasped object. Additionally, we formulate holonomic and nonholonomic constraints generated by two-fingered hand. By represent the Lagrangian for the handling system that includes the constraints and elastic potential energy induced by the deformation of the fingertip, we obtain the equations of motion of the grasped object during the

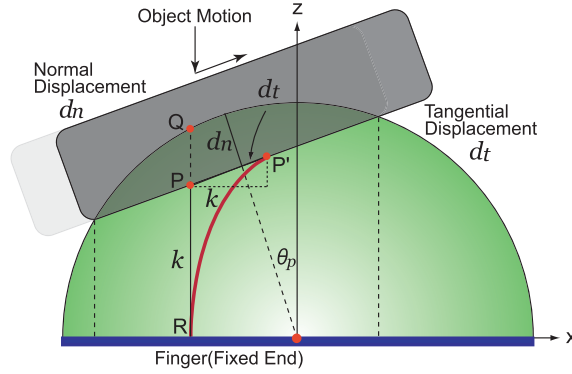


Figure 5.1: Contact mechanism during the soft-fingered manipulation

soft-fingered manipulation. Finally, we simulate the dynamic behavior of the object in the case that both fingers arbitrary move according to an example motion. We clarify that the stable soft-fingered manipulation without any object information can readily be attained under the gravity force.

5.1 Two-dimensional Elastic Model of Soft Fingertip

In what follows, we assume that the slip motion between the object and the fingertip does not occur in all manipulation processes. Before formulating the elastic energy combined by both fingertips in actual two-fingered manipulation, we first describe the energy function in the case of a single contact between the object and a soft fingertip shown in Figure 5.1.

Let Q and R be the opposite end points of a cylindrical virtual spring within the fingertip, and P be a point on the contacting surface. In addition, let k be the spring constant of the cylindrical component, and θ_p be the object orientation in this contact. When the point P shifts d_t from the original point to P' with constant normal displacement d_n , each force for vertical and parallel directions to the fixed end can be represented as follows:

$$dF_v = k(PQ - d_t \sin \theta_p), \quad (5.1)$$

$$dF_p = kd_t \cos \theta_p, \quad (5.2)$$

where we are assuming that the spring constant k is equivalent to that of bending motion. The elastic potential energy induced by the integrated deformation of the compression and bending is therefore expressed by

$$P = \frac{1}{2} \int_{ell} k \left\{ (PQ - d_t \sin \theta_p)^2 + d_t^2 \cos^2 \theta_p \right\}, \quad (5.3)$$

where ell denotes an elliptical region obtained by projecting the contact surface onto the finger plane, as shown in Figure 5.1. Developing Eq.(5.3) with the use of numerical analysis, the energy equation P can finally be represented as

$$P = \pi E \left\{ \frac{d_n^3}{3 \cos^2 \theta_p} - d_n^2 d_t \tan \theta_p + d_n d_t^2 \right\}, \quad (5.4)$$

where E denotes the Young's modulus of the material of the fingertips. Extending the above procedure to the two-fingered hand shown in Figure 5.2, P is then expressed by

$$P = \pi E \sum_{i=1}^2 \left\{ \frac{d_{ni}^3}{3 \cos^2 \theta_{pi}} + (-1)^i d_{ni}^2 d_{ti} \tan \theta_{pi} + d_{ni} d_{ti}^2 \right\}, \quad (5.5)$$

where i means i -th finger of the hand in which 1 and 2 stand for right and left fingers, respectively, and

$$\theta_{pi} = \theta_i + \theta_{obj}. \quad (5.6)$$

5.2 Holonomic and Nonholonomic Constraints

5.2.1 Normal Constraints

As illustrated in Figure 5.2, let W_{obj} be the width of a grasped object, $2W_{fi}$ be the distance between both roots of the fingers, $2d_{fi}$ be the thickness of the finger, (θ_1, θ_2) be the rotational joint angles, L be the length of the finger, and G be the center of gravity of the object. Additionally, let $(x_{obj}, y_{obj}, \theta_{obj})$ be the position and orientation of the object. Considering

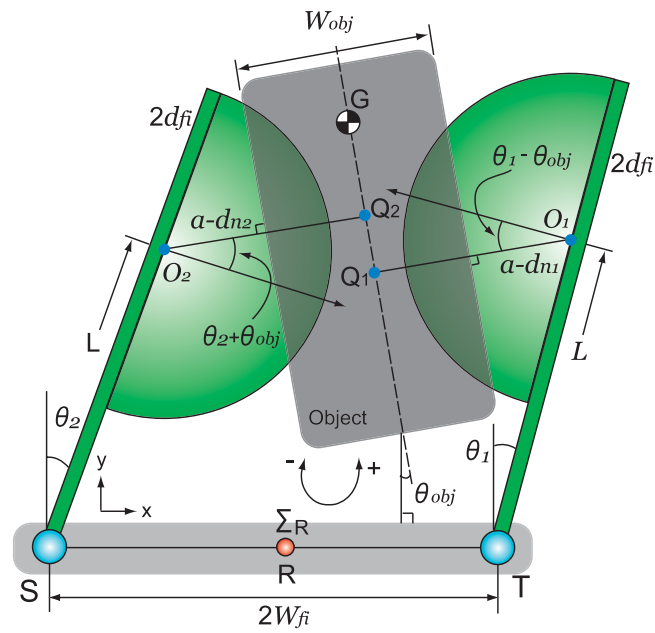


Figure 5.2: Soft-fingered manipulation under the gravitational force

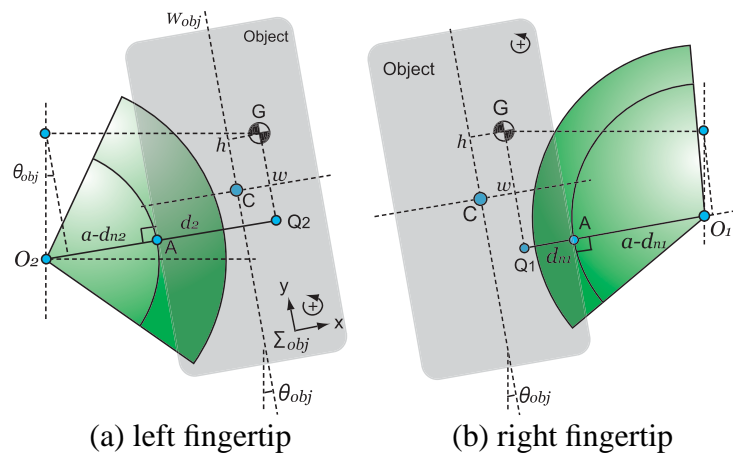


Figure 5.3: Geometric relationship between grasped object and both fingertips

the geometric relationship of the handling system shown in Figure 5.2, the coordinate of the fingertip center O_i is expressed with respect to Σ_R as follows:

$$O_{ix} = (-1)^{i+1}W_{fi} + (-1)^i L \sin \theta_i + (-1)^i d_{fi} \cos \theta_i, \quad (5.7)$$

$$O_{iy} = L \cos \theta_i - d_{fi} \sin \theta_i. \quad (5.8)$$

The constraints along the normal direction to the object surface are holonomic equations, and these can be written by

$$\begin{aligned} C_i^H &= (-1)^i (x_{obj} - O_{ix}) \cos \theta_{obj} \\ &+ (-1)^i (y_{obj} - O_{iy}) \sin \theta_{obj} \\ &- (a - d_{ni}) + \frac{W_{obj}}{2} + (-1)^i w = 0. \end{aligned} \quad (5.9)$$

In this paper, we give essentric distances (w, h) of point G to be zero for ease of explanation, and θ_{obj} has a positive value in the counter-clockwise direction.

5.2.2 Tangential Constraints

Letting θ_i be positive when both fingers rotate inward as shown in Figure 5.2, the rolling velocity \dot{s}_i of the object on the soft fingertip is expressed as

$$\dot{s}_i = -(a - d_i) \left\{ \dot{\theta}_i + (-1)^i \dot{\theta}_{obj} \right\}. \quad (5.10)$$

In addition, as illustrated in Figure 5.3, the distance GQ_i is represented as

$$GQ_i = -(x_{obj} - O_{ix}) \sin \theta_{obj} + (y_{obj} - O_{iy}) \cos \theta_{obj}. \quad (5.11)$$

Therefore, differentiating Eq.(5.11) with respect to time, a velocity constraint including the change of bending motion \dot{d}_{ti} can be given as a nonholonomic constraint:

$$C_i^N = G\dot{Q}_i - \dot{s}_i + \dot{d}_{ti} = 0. \quad (5.12)$$

5.3 General Description of Equations of Motion

In this study, we deal with the soft-fingered manipulation using a minimum degrees of freedom hand, and investigate the dynamic behavior of a grasped known object in the case of the presence of holonomic and nonholonomic constraints in the system.

5.3.1 Lagrangian

Let \mathbf{q} be the generalized coordinate, (M_{obj}, I_{obj}) be the mass and moment of inertia of the grasped object respectively, and $\mathbf{I} = [I_1, I_2]^T$ be the moment of inertia of both fingers. In addition, let g be the acceleration of gravity, P_{gv} be the potential energy with respect to gravitational force, λ_i^H be the constraint force in terms of the holonomic constraint C_i^H expressed in Eq.(5.9). The Lagrangian in the present handling system can then be described using Eq.(5.5) as

$$L = \frac{1}{2} \dot{\mathbf{q}}^T \mathbf{M} \dot{\mathbf{q}} - P - P_{gv} + \sum_{i=1}^2 \lambda_i^H C_i^H, \quad (5.13)$$

where

$$\mathbf{M} = \text{diag}(M_{obj}, M_{obj}, I_{obj}, \mathbf{I}^T, M_{obj}, M_{obj}, M_{obj}, M_{obj}) \in \mathbf{R}^{9 \times 9}, \quad (5.14)$$

$$\mathbf{q} = [x_{obj}, y_{obj}, \theta_{obj}, \boldsymbol{\theta}_i^T, \mathbf{d}_{ni}^T, \mathbf{d}_{ti}^T]^T \in \mathbf{R}^{9 \times 1}, \quad (5.15)$$

$$P_{gv} = M_{obj} g y_{obj}. \quad (5.16)$$

In Eq.(5.13), the first term means the kinetic energy in the entire system, and the second and third terms stand for the elastic potential energy of the soft fingers and gravitational potential energy. In addition, the last term denotes a virtual energy due to the constraint forces that does not generate any energy, that is, it always be zero.

5.3.2 Equations of Motion

As expressed as Eqs.(5.9) and (5.12), this handling system has four constraint equations that is associated with normal and tangential directions to the grasped object. Note that while the holonomic constraints can be included into the Lagrangian directly, we are able to contain the nonholonomic constraints into the equations of motion for the first time [26].

We define the nonholonomic constraint matrix as $\Phi^N \in R^{2 \times 9}$ [27]. The element of the matrix is then expressed using Eq.(5.12) as

$$\Phi_{ij}^N = \frac{\partial C_i^N}{\partial \dot{q}_j} \quad (i = 1, 2 : j = 1, \dots, 9). \quad (5.17)$$

Let $\lambda^N = [\lambda_1^N, \lambda_2^N]^T$ be the constraint force vector directed to the tangential direction to the object surface. As long as $\Phi^{NT} \lambda^N$ is represented as a linear combination form relating to the time derivative of generalized coordinate, the equations of motion under nonholonomic constraints can be expressed as [26]

$$\frac{d}{dt} \frac{\partial L}{\partial \dot{q}_j} - \frac{\partial L}{\partial q_j} = \Phi^{NT} \lambda^N \quad (j = 1, \dots, 9). \quad (5.18)$$

5.3.3 Constraint Stabilization Method including Nonholonomic Constraints

In order to investigate the dynamic analysis of a system under both kinds of constraints, we apply the *Constraint Stabilization Method* (CSM) [28] in this study.

Let C^H, C^N be the vector description of Eqs.(5.9) and (5.12). Here, corrected constraint equations that is based on each constraint are described as

$$\ddot{C}^H + 2\alpha\dot{C}^H + \alpha^2 C^H = \mathbf{0} \in R^{2 \times 1}, \quad (5.19)$$

$$\dot{C}^N + \beta C^N = \mathbf{0} \in R^{2 \times 1}, \quad (5.20)$$

where α, β correspond to an arbitrary constant associated with the speed of asymptotical stability of both equations. By using Eqs.(5.19) and (5.20) in the numerical analysis of corresponding equations of motion, we can obtain the solution of the system stably.

On the other hand, let $\Phi^H \in R^{2 \times 9}$ be the holonomic constraint matrix of the system as well. Each element of the matrix is then expressed using Eq.(5.9) as

$$\Phi_{ij}^H = \frac{\partial C_i^H}{\partial q_j} \quad (i = 1, 2 : j = 1, \dots, 9). \quad (5.21)$$

By developing Eqs.(5.19) and (5.20) with both constraint matrices Φ^H and Φ^N , we can define γ^H and γ^N as follows:

$$\Phi^H \dot{\mathbf{p}} = -\mathbf{b}^H(\mathbf{q}, \mathbf{p}) - 2\alpha \dot{\mathbf{C}}^H - \alpha^2 \mathbf{C}^H \triangleq -\gamma^H, \quad (5.22)$$

$$\Phi^N \dot{\mathbf{p}} = -\mathbf{b}^N(\mathbf{q}, \mathbf{p}) - \beta \mathbf{C}^N \triangleq -\gamma^N, \quad (5.23)$$

where \mathbf{p} denotes the generalized velocity vector, and the relationship $\mathbf{p} = \dot{\mathbf{q}}$ is also satisfied. Note that in the above process we separate *dot description* (generalized acceleration: $\dot{\mathbf{p}}$) and *dot-free description* (generalized coordinate and velocity: \mathbf{q} and \mathbf{p}) across the equal sign.

Furthermore, let \mathbf{f}_p be the potential force vector, \mathbf{f}_{ext} be the vector of generalized external force, and \mathbf{I} be the identity matrix. The state space description of the CSM including a control input vector \mathbf{u}_{IN} , which is able to deal with the holonomic and nonholonomic constraints simultaneously, is described as [29, 30]

$$\begin{bmatrix} \mathbf{I} & \mathbf{0} & \mathbf{0} & \mathbf{0} \\ \mathbf{0} & \mathbf{M} & -\Phi^{HT} & -\Phi^{NT} \\ \mathbf{0} & -\Phi^H & \mathbf{0} & \mathbf{0} \\ \mathbf{0} & -\Phi^N & \mathbf{0} & \mathbf{0} \end{bmatrix} \begin{bmatrix} \dot{\mathbf{q}} \\ \dot{\mathbf{p}} \\ \lambda^H \\ \lambda^N \end{bmatrix} = \begin{bmatrix} \mathbf{p} \\ \mathbf{f}_p + \mathbf{f}_{ext} + \mathbf{u}_{IN} \\ \gamma^H \\ \gamma^N \end{bmatrix}. \quad (5.24)$$

By developing Eq.(5.24) with respect to $\dot{\mathbf{p}}$, we obtain the equations of motion with respect to all the generalized coordinates represented in Eq.(5.15).

5.4 E.O.Ms for Dynamic Manipulation

We formulate the equations of motion of the handling system illustrated in Figure 5.2 in a concrete form. First, we show the constraint matrices that appear along the normal and

tangential direction to the object surface, and nonlinear equations of motion of the system. In what follows, we describe the equations of motion with respect to the object position (x_{obj}, y_{obj}) and orientation θ_{obj} , and also represent other equations with respect to the rotational angle of the finger θ_i and fingertip displacement (d_{ni}, d_{ti}) .

5.4.1 Constraint Matrix

The constraint matrix $\Phi = [\Phi^{HT}, \Phi^{NT}]^T \in R^{4 \times 9}$ including both holonomic and nonholonomic constraints in the present handling system can be expressed using Eqs.(5.9), (5.12), (5.17), and (5.21) as

$$\Phi = \begin{bmatrix} -C\theta_{obj} & -S\theta_{obj} & A_{c1} & B_{c1} & 0 & 1 & 0 & 0 & 0 \\ C\theta_{obj} & S\theta_{obj} & A_{c2} & 0 & B_{c2} & 0 & 1 & 0 & 0 \\ -S\theta_{obj} & C\theta_{obj} & E_{c1} & F_{c1} & 0 & 0 & 0 & 1 & 0 \\ -S\theta_{obj} & C\theta_{obj} & E_{c2} & 0 & F_{c2} & 0 & 0 & 0 & 1 \end{bmatrix}. \quad (5.25)$$

In Eq.(5.25), the symbols S and C denote the abbreviation of *sin* and *cos*, respectively. Additionally, $A_{ci}, B_{ci}, E_{ci}, F_{ci}$ ($i = 1, 2$) correspond to the following equations.

$$A_{ci} = (-1)^{i+1}(x_{obj} - O_{ix})S\theta_{obj} + (-1)^i(y_{obj} - O_{iy})C\theta_{obj}, \quad (5.26)$$

$$B_{ci} = -LC \left\{ \theta_i + (-1)^i \theta_{obj} \right\} + d_{fi} S \left\{ \theta_i + (-1)^i \theta_{obj} \right\}, \quad (5.27)$$

$$E_{ci} = -(x_{obj} - O_{ix})C\theta_{obj} - (y_{obj} - O_{iy})S\theta_{obj} + (-1)^i(a - d_{ni}), \quad (5.28)$$

$$F_{ci} = LS \left\{ \theta_r + (-1)^i \theta_{obj} \right\} + d_{fi} C \left\{ \theta_i + (-1)^i \theta_{obj} \right\} + (a - d_{ni}), \quad (5.29)$$

where A_{ci} corresponds to $(-1)^i GQ_i$ as shown in Eq.(5.11) and Figure 5.3, and B_{ci} stands for the tangential component of position vector from each origin T, S of the i -th finger to each origin O_i of the i -th fingertip, as shown in Figure 5.2. Furthermore, F_{ci} means the normal component of position vector from each origin T, S of the i -th finger to the center of the contacting circle on the fingertip. E_{ci} can be transformed using Eq.(5.9) into a constant expression:

$$E_{ci} = -(-1)^i \frac{W_{obj}}{2} - w. \quad (5.30)$$

5.4.2 Equations of Motion

By developing Eq.(5.18), the equations of motion relating to all the system variables can be presented as

$$M_{obj}\ddot{x}_{obj} + \boldsymbol{\lambda}^T \mathbf{s}_x = 0, \quad (5.31)$$

$$M_{obj}\ddot{y}_{obj} + \boldsymbol{\lambda}^T \mathbf{s}_y = 0, \quad (5.32)$$

$$I_{obj}\ddot{\theta}_{obj} + A + B - \boldsymbol{\lambda}^T \mathbf{s}_\theta = 0, \quad (5.33)$$

$$I_i\ddot{\theta}_i - \frac{2\pi E d_{ni}^3 \sin\{\theta_i + (-1)^i \theta_{obj}\}}{3 \cos^3\{\theta_i + (-1)^i \theta_{obj}\}} + \frac{\pi E d_{ni}^2 d_{ti}}{\cos^2\{\theta_i + (-1)^i \theta_{obj}\}} - \lambda_i^H B_{ci} - \lambda_i^N F_{ci} = u_{INi}, \quad (5.34)$$

$$M_{obj}\ddot{d}_{ni} + \frac{\pi E d_{ni}^2}{\cos^2\{\theta_i + (-1)^i \theta_{obj}\}} + 2\pi E d_{ni} d_{ti} \tan\{\theta_i + (-1)^i \theta_{obj}\} + \pi E d_{ti}^2 - \lambda_i^H + c_n \dot{d}_{ni} = 0, \quad (5.35)$$

$$M_{obj}\ddot{d}_{ti} + \pi E d_{ni}^2 \tan\{\theta_i + (-1)^i \theta_{obj}\} + 2\pi E d_{ni} d_{ti} - \lambda_i^N + c_t \dot{d}_{ti} = 0, \quad (5.36)$$

where $\boldsymbol{\lambda} = [\lambda_1^H, \lambda_2^H, \lambda_1^N, \lambda_2^N]^T$ and $A, B, \mathbf{s}_x, \mathbf{s}_y, \mathbf{s}_\theta$ correspond to the following equations:

$$A = \frac{2\pi E}{3} \left\{ \frac{d_{n1}^3 \mathbf{S}(\theta_1 - \theta_{obj})}{\mathbf{C}^3(\theta_1 - \theta_{obj})} - \frac{d_{n2}^3 \mathbf{S}(\theta_2 + \theta_{obj})}{\mathbf{C}^3(\theta_2 + \theta_{obj})} \right\}, \quad (5.37)$$

$$B = \pi E \left\{ \frac{-d_{n1}^2 d_{t1}}{\mathbf{C}^2(\theta_1 - \theta_{obj})} + \frac{d_{n2}^2 d_{t2}}{\mathbf{C}^2(\theta_2 + \theta_{obj})} \right\}, \quad (5.38)$$

$$\mathbf{s}_x = [\mathbf{C}\theta_{obj}, -\mathbf{C}\theta_{obj}, \mathbf{S}\theta_{obj}, \mathbf{S}\theta_{obj}]^T, \quad (5.39)$$

$$\mathbf{s}_y = [\mathbf{S}\theta_{obj}, -\mathbf{S}\theta_{obj}, -\mathbf{C}\theta_{obj}, -\mathbf{C}\theta_{obj}]^T, \quad (5.40)$$

$$\mathbf{s}_\theta = [A_{c1}, A_{c2}, E_{c1}, E_{c2}]^T. \quad (5.41)$$

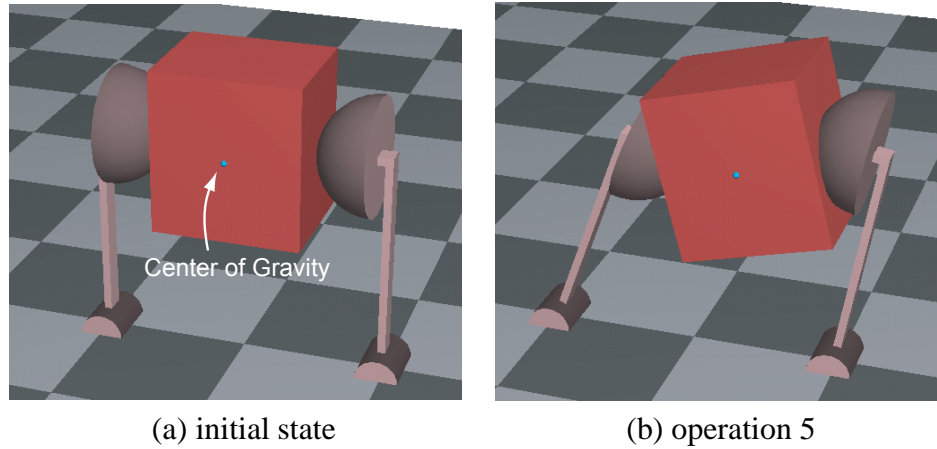


Figure 5.4: Snapshots on simulation

5.5 Simulation

In this paper, we clarify that the stable grasping and manipulation using the soft-fingered hand can consistently be achieved steadily. In what follows, we consider an example motion of the hand, and simulate the dynamic behavior of the grasped object expressed as Eqs.(5.31), (5.32), and (5.33) during the given manipulating motion.

5.5.1 Example Motion

The example motion of the fingers, which is dealt with in this study, is as follows:

1. Initial state: Both fingers grasp an object in parallel (Figure 5.4-(a))
2. Motion 1: $(\theta_1^d, \theta_2^d) = (6 \text{ deg}, 6 \text{ deg})$
3. Motion 2: $(\theta_1^d, \theta_2^d) = (20 \text{ deg}, -10 \text{ deg})$
4. Motion 3: $(\theta_1^d, \theta_2^d) = (-2 \text{ deg}, 13 \text{ deg})$
5. Motion 4: $(\theta_1^d, \theta_2^d) = (-10 \text{ deg}, 20 \text{ deg})$
6. Motion 5: $(\theta_1^d, \theta_2^d) = (-7 \text{ deg}, 17 \text{ deg})$ (Figure 5.4-(b))
7. Motion 6: $(\theta_1^d, \theta_2^d) = (17 \text{ deg}, -7 \text{ deg})$

Table 5.1: Simulation parameters

| Parameters | Values |
|------------------------------|------------------------|
| Rungekutta sampling time | 0.1 msec |
| α | 20000 |
| β | 10000 |
| P-Gain : K_P | 300 |
| D-Gain : K_D | 14 |
| I-Gain : K_I | 0.1 |
| Viscosity for $d_{ni} : c_n$ | 300 Ns/m |
| Viscosity for $d_{ti} : c_t$ | 300 Ns/m |
| L | 76.2 mm |
| $2W_{fi}$ | 97 mm |
| a | 20 mm |
| W_{obj} | 49 mm |
| M_{obj} | 0.3 kg |
| I_{obj}, I_1, I_2 | 125 kg·mm ² |
| d_{fi} | 4 mm |
| Young's modulus : E | 0.232 MPa |

8. Motion 7: $(\theta_1^d, \theta_2^d) = (-15 \text{ deg}, 25 \text{ deg})$

9. Motion 8: $(\theta_1^d, \theta_2^d) = (5 \text{ deg}, 5 \text{ deg})$

As shown in Figure 5.4-(a), the fingers are positioned in the initial state so that geometric point-contact between the object and soft fingers is maintained. After the operation 1, we perform a feedback control with respect to the rotational angle θ_i according to the above desired angle of the finger. A PID control law is applied to the present system, and it is described as

$$u_{INi} = -K_P(\theta_i - \theta_i^d) - K_D\dot{\theta}_i - K_I \int_0^t (\theta_i - \theta_i^d) d\tau. \quad (5.42)$$

In this system, we do not consider any disturbance, and also set that the external force is zero in Eq.(5.24) such that $\mathbf{f}_{ext} = \mathbf{0}$. We input Eq.(5.42) into \mathbf{u}_{IN} expressed in Eq.(5.24) as a torque command. Parameters in the numerical analysis are given in Table 5.1. Also, Mechanical parameters used for the two-fingered hand are given in Table 5.1.

5.5.2 Results

Figure 5.5-(a) and (b) show the results of trajectory of both fingers, and Figure 5.5-(c), (d), and (e) show the object position and orientation with respect to time, respectively. As shown in all the figures in Figure 5.5, the resultant force and moment induced by the elastic deformation of the soft fingers consistently keep the manipulating motion stable. In other words, we can find that the position and orientation converge to a certain state determined by the force-moment equilibrium on the soft fingertips.

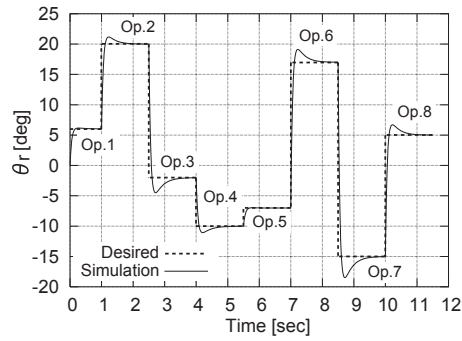
In addition, we evaluate whether the CSM containing both constraints works well in the numerical analysis. That is, we verify that each constraint equation expressed as Eqs.(5.9) and (5.12) converges to zero during the computation. Figure 5.6-(a) and (b) show the error value of normal constraint on the i -th fingertip, and Figure 5.6-(c) and (d) show that of tangential constraint.

In the result of holonomic constraint C_i^H , we find that the numerical order plotted on y -axis becomes approximately 10^{-8} , and as a result, Eq. (5.9) is satisfied in the numerical computation. In the case of nonholonomic constraint, we know that the value on each switching point of the individual operation relatively increases at one point. This results from the fact that the time derivative of rotational angle $\dot{\theta}_i$ becomes substantially large value in the simulation due to the step inputs in all operations, as shown in Figure 5.5-(a) and (b). At the same time, the numerical order along y -axis exhibits 10^{-6} except the switching points. As a result, we can conclude that the CSM including holonomic and nonholonomic constraints works well in the numerical simulation.

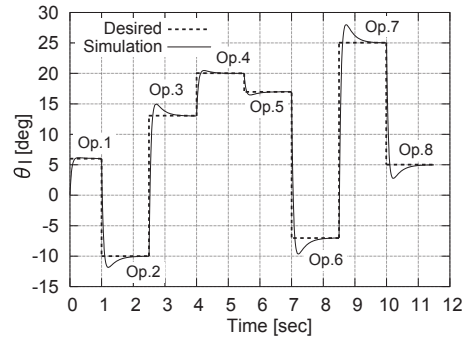
5.6 Concluding Remarks

In this study, we have first formulated a two-dimensional fingertip model that contains the compression and bending motion simultaneously. Also we have simulated the dynamic behavior of a parallel-rigid object grasped by a minimum dof soft-fingered hand. In this process, we have applied an extended CSM that includes holonomic and nonholonomic constraints induced by the soft-fingered manipulation.

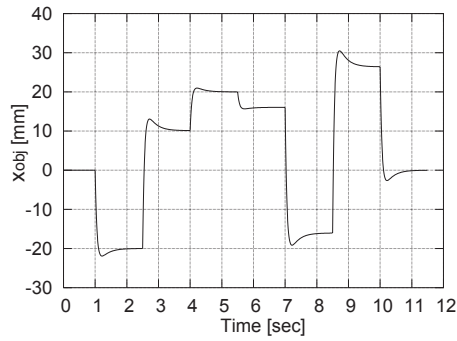
This study indicates that soft-fingered manipulation is able to simply achieve secure



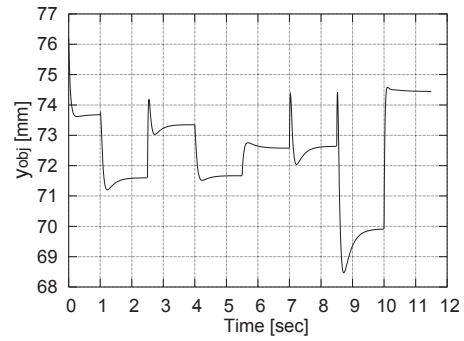
(a) θ_1 vs. time



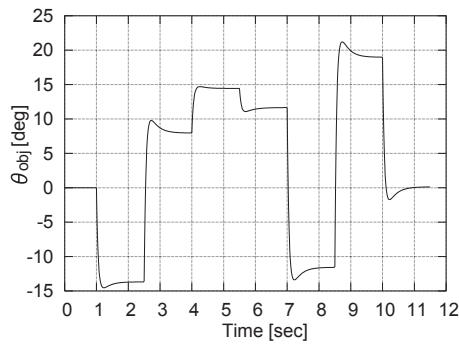
(b) θ_2 vs. time



(c) x_{obj} vs. time



(d) y_{obj} vs. time



(e) θ_{obj} vs. time

Figure 5.5: Simulation results of object position and orientation

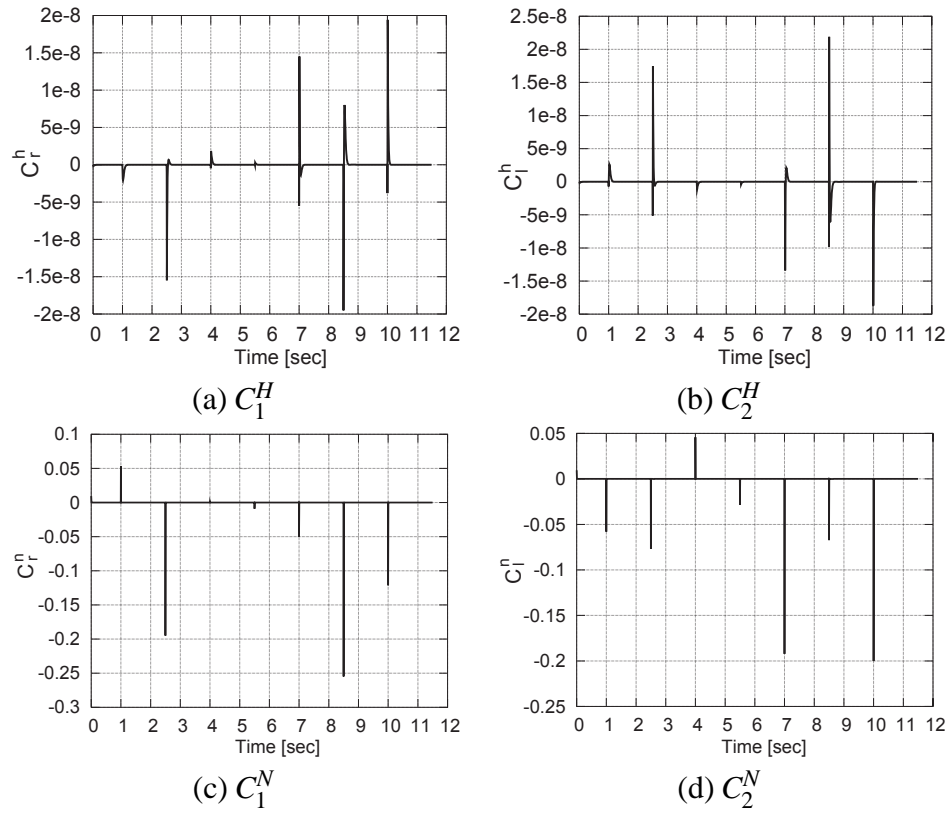


Figure 5.6: Convergence of four constraints

grasping and robust manipulation even when we actuate two fingers freely without any object information, which is called "*Blind Manipulation*". We have clarified that the flexibility of soft fingertips greatly contributes to stable grasping and manipulation.

Chapter 6

Conclusions

This thesis has first proposed a simple contact mechanism between a pair of soft fingertips and a rigid grasped object by two-fingered hand, which is based on physical perspective and material mechanics. In the process, we have found a new experimental finding that a minimum point of elastic potential energy appears due to the deformation of a hemispherical soft fingertip. The experimental knowledge can also be found in the contact model formulated in Chapters 3 and 4, and we call it "Local Minimum of Elastic Potential Energy", abbreviated as LMEE.

In Chapter 4, we have analyzed an LMEE-based quasi-static manipulation. By focusing on the static behavior of an object grasped by two-fingered robotic hand, we have verified that the LMEE works well in the soft-fingered handling.

Finally in Chapter 5, we have represented equations of motion of a minimum degrees of freedom handling system in a dynamic sense, and clarified that the robust manipulation by soft fingers can consistently be achieved against free motions of the robotic fingers even in a simple control scheme.

In future works, we need to investigate the stability of soft-fingered manipulation in an analytical way, and also design the control law to realize the simultaneous force and posture control of a grasped object via a minimum degrees of freedom robotic hand.

Appendix A

Contact Plane Formula

As illustrated in Figure 5.1, the point C is described in a vector form as

$$\vec{OC} = \begin{bmatrix} (a-d) \sin \theta_p \\ 0 \\ (a-d) \cos \theta_p \end{bmatrix}. \quad (\text{A.1})$$

In addition, a normal unit vector with respect to the contact surface is represented as

$$\mathbf{n} = \begin{bmatrix} \sin \theta_p \\ 0 \\ \cos \theta_p \end{bmatrix}. \quad (\text{A.2})$$

Since the contact plane can be written by an inner product form, $\{[x, y, z]^T - \vec{OC}\} \cdot \mathbf{n} = 0$, the plane equation is therefore described as follows:

$$x \sin \theta_p + z \cos \theta_p = a - d. \quad (\text{A.3})$$

Appendix B

Spring Constant Formulation

As shown in Figure B.1, letting k_0 , dS_0 , and L_0 respectively be the spring constant, the sectional area, and the natural length of a specimen for measuring the Young's modulus, and E be the Young's modulus obtained from an appropriate compression test, we can write and develop following equations according to linear material mechanics:

$$\sigma = E\varepsilon \quad (\text{B.1})$$

$$\Leftrightarrow \frac{F}{S_0} = E \frac{\delta x}{L_0} \quad (\text{B.2})$$

$$\Leftrightarrow E = \frac{L_0}{\delta x} \cdot \frac{F}{S_0} = \frac{L_0}{\delta x} \cdot \frac{k_0 \delta x}{S_0} = k_0 \frac{L_0}{S_0}, \quad (\text{B.3})$$

where F denotes an applied force to the specimen and δx is a displacement in the identification test. Since this paper assumes that the Young's modulus is an invariant physical value for individual material, the following equation is satisfied:

$$k \frac{L}{dS} = k_0 \frac{L_0}{S_0} = E \quad (\text{B.4})$$

$$\Leftrightarrow k = E \frac{dS}{L} = \frac{EdS}{\sqrt{a^2 - (x^2 + y^2)}}. \quad (\text{B.5})$$

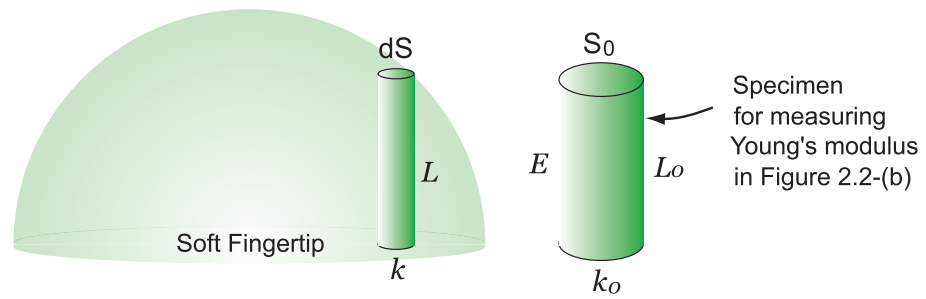


Figure B.1: Spring constant inside the soft fingertip.

Appendix C

Coordinate Conversion to Derive the Fingertip Stiffness

As illustrated in Figure C.1, let Σ' be the coordinate system translated to O' from the Σ frame, and Σ'' be the cylindrical coordinate system inclined by θ_p from z' -axis. Let r be the arbitrary radius on the contact circle that has an origin C , and ϕ be the common rotational angle around the z -, z' -, and z'' -axes. The relationship between (x', y') on the Σ' frame and (r, ϕ) on the Σ'' frame is then expressed as

$$x' = r \cos \phi \cos \theta_p, \quad (\text{C.1})$$

$$y' = r \sin \phi. \quad (\text{C.2})$$

Since the relationship between (x, y) and (x', y') is described as $x = x' + (a - d) \sin \theta_p$ and $y = y'$, the variable transformation through the coordinate systems Σ and Σ'' can be expressed as

$$x = r \cos \phi \cos \theta_p + (a - d) \sin \theta_p, \quad (\text{C.3})$$

$$y = r \sin \phi. \quad (\text{C.4})$$

Simultaneously, the elliptical region at the bottom surface of the fingertip shown in Figure C.1 can be converted to a circular region according to the above transformation rule, that

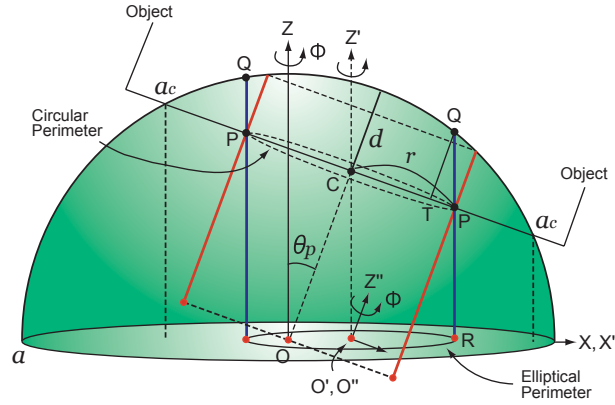


Figure C.1: Equivalent fingertip stiffness with respect to Σ'' -coordinate system.

is, the integration area of (r, ϕ) varies at $[0, a_c]$ and $[0, 2\pi]$, respectively.

Next, let us consider the physical meaning of the double integration of $B(r, \phi)$ used in Eqs. (2.9) and (2.13), which is detailed in Eq. (2.6) as:

$$\int_0^{2\pi} B(r, \phi) d\phi = \int_0^{2\pi} \frac{\cos \theta_p d\phi}{\sqrt{a^2 - \{x^2(r, \phi) + y^2(r, \phi)\}}}. \quad (\text{C.5})$$

Eq. (C.5) corresponds to a stiffness on an elliptical perimeter whose longitudinal radius is r , as shown in Figure C.2-(a). Additionally, substituting θ_p into Eq. (C.5) enables to obtain an equivalent stiffness on a circular perimeter of radius r shown in Figure C.2-(b).

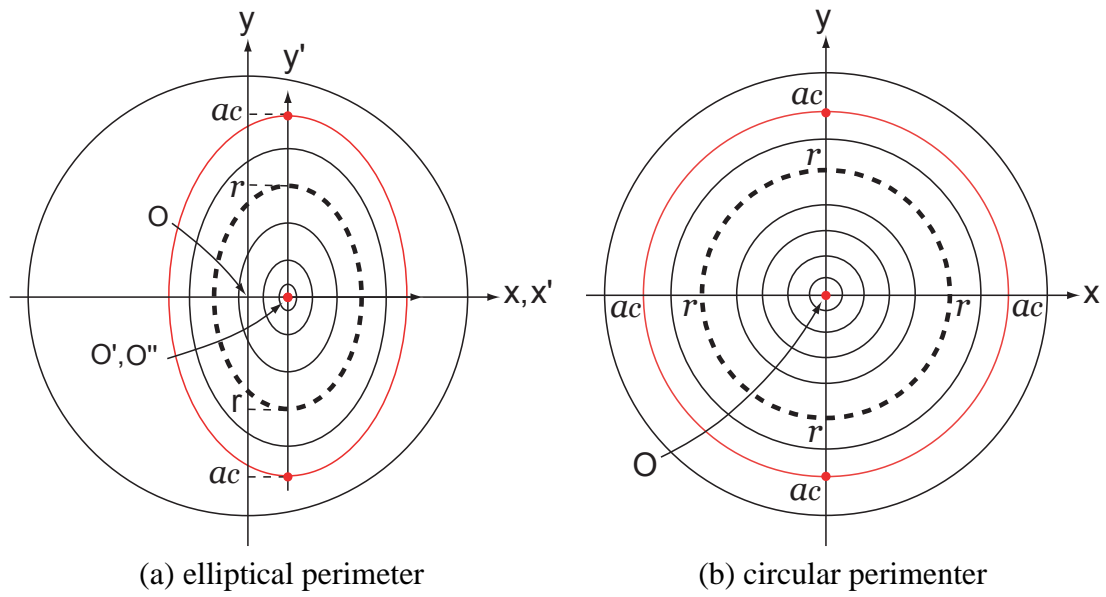


Figure C.2: Fingertip stiffness on a certain perimeter.

Appendix D

Relationship between Elastic Force and Potential Energy

While the individual virtual spring used in our study is based on a linear elasticity, the entire fingertip model that is obtained by completing the double integration on an elliptical region exhibits a geometrical nonlinearity caused by the hemispherical shape of the fingertip. In other words, the completed fingertip model has a nonlinear fingertip stiffness expressed as Eq. (2.7). Hence, when we compute the total force Eq. (2.11) from the energy Eq. (2.14), we must define an *equivalent displacement* and use it for the differential calculation.

In the case of normal contact that corresponds to $\theta_p = 0$, elastic models are given as follows:

$$P = \frac{\pi E d^3}{3}, \quad (\text{D.1})$$

$$\frac{\partial P}{\partial d} = \pi E d^2 = F, \quad (\text{D.2})$$

$$\frac{\partial^2 P}{\partial d^2} = 2\pi E d = K, \quad (\text{D.3})$$

where d itself corresponds to the equivalent displacement.

Continuously, let us consider the case of diagonal contact when $\theta_p \neq 0$. We define Δz_{eq}

as an equivalent displacement, and it must satisfy

$$\frac{\partial P}{\partial \Delta z_{eq}} = \frac{\pi E d^2}{\cos \theta_p} = F, \quad (\text{D.4})$$

$$\frac{\partial^2 P}{\partial \Delta z_{eq}^2} = 2\pi E d = K. \quad (\text{D.5})$$

The displacement Δz_{eq} to fulfill Eqs. (D.4) and (D.5) can be found such that a geometrical relationship $d = \Delta z_{eq} \cos \theta_p$ is maintained as shown in Figure C.1. It is obvious that Δz_{eq} means a true maximum displacement among all the virtual springs in any case that includes $\theta_p = 0$ and $\theta_p \neq 0$.

Appendix E

Approximation Method for Nonlinear Curve

As shown in Figure 3.2-(b), the stress-strain curve obtained by averaging six raw data depicted in Figure 3.2-(a) passes through an original point on the figure. We therefore introduce a stress formula that does not include constant terms as follows:

$$\sigma(\varepsilon) = \sum_{i=1}^n a_i \varepsilon^i. \quad (\text{E.1})$$

In what follows we determine the maximum order n and the constant a_i used in Eq. (E.1). For comparison, we apply several model functions of $n = 3, 4, 5, 6, 7$ into Eq. (E.1), and plot each approximated result of the functions on Table E.1. Note that ASE [%] means Asymptotical Standard Error and it corresponds to a standard error of each constant a_i . Furthermore, RSME denotes an root-mean-square value of the error, and it is used for Least-Squares Method as a dimensionless index to evaluate the level of approximation. For example, as the RSME of a result obtained in some test gets closer to zero, the result becomes more good approximation.

As shown in Table E.1, the ASEs become comparatively large value in the approximated result given in the column of the third-order and fourth-order equations. On the contrary, the ASEs decrease rapidly in the approximated results over the fifth-order equation. Furthermore, in the results of sixth-order and seventh-order equations, while we get

Table E.1: Asymptotical standard error

| | 3 | 4 | 5 | 6 | 7 |
|--------------|---------|---------|------------|------------|------------|
| ASE(a_1) | 2.94 | 4.132 | 4.223e-7 | 6.753e-7 | 1.012e-6 |
| ASE(a_2) | 2.307 | 1.977 | 5.48e-7 | 1.232e-6 | 2.463e-6 |
| ASE(a_3) | 1.501 | 1.449 | 3.236e-7 | 1.078e-6 | 2.963e-6 |
| ASE(a_4) | | 0.9937 | 2.187e-7 | 1.202e-6 | 4.806e-6 |
| ASE(a_5) | | | 1.396e-7 | 1.674e-6 | 1.088e-5 |
| ASE(a_6) | | | | 71.43 | 67.42 |
| ASE(a_7) | | | | | 72.11 |
| RMSE | 27.1249 | 7.32683 | 2.88568e-7 | 2.88394e-7 | 2.88227e-7 |

good results up to a_5 , the ASEs tend to increase in a_6, a_7 .

On the other hand, the RMSEs are comparatively large in the third-order and fourth-order approximations, but it exhibits extremely small value over the fifth-order. After that, it remains at low level of the value. Thus, the approximation method is valid for computing a nonlinear Young's modulus of the soft fingertip, and the fifth-order stress-strain curve obtained in the approximation, which is represented as Eq. (3.3), is well-fitted to an averaged curve shown in Figure 3.2-(b).

Bibliography

- [1] Y.Yokokohji, M.Sakamoto, and T.Yoshikawa, "Vision-Aided Object Manipulation by a Multifingered Hand with Soft Fingertips" *Proc. IEEE Int. Conf. on Robotics and Automation*, Detroit, Michigan, pp.3201-3208, May, 1999.
- [2] Y.Yokokohji, M.Sakamoto, and T.Yoshikawa, "Object Manipulation by Soft Fingers and Vision" *Proc. 9th Int. Symposium of Robotics Research*, Snowbird, Utah, pp.365-374, Oct., 1999.
- [3] H.Maekawa, K.Komoriya, and K.Tanie, "Manipulation of an Unknown Object by Multifingered Hands with Rolling Contact Using Tactile Feedback" *Proc. IEEE Int. Conf. on Intelligent Robots and Systems*, Raleigh, North Carolina, pp.1877-1882, July, 1992.
- [4] H.Maekawa, K.Tanie, K.Komoriya, M.Kaneko, C.Horiguchi, and T.Sugawara, "Development of a Finger-Shaped Tactile Sensor and its Evaluation by Active Touch" *Proc. IEEE Int. Conf. on Robotics and Automation*, Nice, France, pp.1327-1334, May, 1992.
- [5] S.Arimoto, P.Nguyen, H.Y.Han, and Z.Doulgeri, "Dynamics and Control of a set of Dual Fingers with Soft Tips", *Robotica*, Vol.18, pp.71-80, 2000.
- [6] S.Arimoto, Z.Doulgeri, P.Nguyen, and J.Fasoulas, "Stable Pinching by a pair of Robot Fingers with Soft Tips under the Effect of Gravity", *Robotica*, Vol.20, pp.241-249, 2002.
- [7] Z.Doulgeri, J.Fasoulas, and S.Arimoto, "Feedback Control for Object Manipulation by a pair of Soft Tip Fingers", *Robotica*, Vol.20, pp.1-11, 2002.

- [8] Z.Doulgeri and J.Fasoulas, "Grasping Control of Rolling Manipulation with Deformable Fingertips", *IEEE/ASME Trans. on Mechatronics*, Vol.8, No.2, pp.283-286, 2003.
- [9] N.Xydas and I.Kao, "Modeling of Contact Mechanics and Friction Limit Surfaces for Soft Fingers in Robotics, with Experimental Results", *Journal of Robotics Research*, Vol.18, No.8, pp.941-950, 1999.
- [10] N.Xydas, M.Bhagavat and I.Kao, "Study of Soft-Finger Contact Mechanics Using Finite Elements Analysis and Experiments", *Proc. IEEE Int. Conf. on Robotics and Automation*, San Francisco, California, pp.2179-2184, April, 2000.
- [11] I.Kao and F.Yang, "Stiffness and Contact Mechanics for Soft Fingers in Grasping and Manipulation", *IEEE Trans. on Robotics and Automation*, Vol.20, No.1, pp.132-135, 2004.
- [12] T.Inoue and S.Hirai, "Modeling of Soft Fingertip for Object Manipulation Using Tactile Sensing", *Proc. IEEE Int. Conf. on Intelligent Robots and Systems*, Las Vegas, Nevada, pp.2654-2659, Oct., 2003.
- [13] T.Inoue and S.Hirai, "Local Minimum of Elastic Potential Energy on Hemispherical Soft Fingertip", *Proc. IEEE Int. Conf. on Robotics and Automation*, Barcelona, Spain, pp.2319-2324, April, 2005.
- [14] S.Hirai and A.Asada, "Kinematics and statics of manipulation using the theory of polyhedral convex cones", *Int. Journal of Robotics Research*, Vol.12, No.5, pp.434-447, 1993.
- [15] R.Murray, Z.Li and S.Sastry, "A mathematical introduction to robotic manipulation", CRC Press, 1999.
- [16] M.Mason, "Mechanics of robotic manipulation", MIT Press, 2001.
- [17] P.Nguyen and S.Arimoto, "Performance of Pinching Motions of Two Multi-DOF Robotic Fingers with Soft-Tips", *Proc. IEEE Int. Conf. on Robotics and Automation*, Seoul, Korea, pp.2344-2349, May, 2001.

- [18] S.Arimoto, K.Tahara, M.Yamaguchi, P.Nguyen, and H.Y.Han, "Principle of Superposition for Controlling Pinch Motions by means of Robot Fingers with Soft Tips", *Robotica*, Vol.19, pp.21-28, 2001.
- [19] J.Fasoulas and Z.Doulgeri, "Equilibrium Conditions of a Rigid Object Grasped by Elastic Rolling Contacts", *Proc. IEEE Int. Conf. on Robotics and Automation*, New Orleans, Louisiana, pp.789-794, April, 2004.
- [20] T.Inoue and S.Hirai, "Quasi-Static Manipulation with Hemispherical Soft Fingertip via Two Rotational Fingers", *Proc. IEEE Int. Conf. on Robotics and Automation*, Barcelona, Spain, pp.1947-1952, April, 2005.
- [21] T.Inoue and S.Hirai, "Study on Hemispherical Soft-Fingered Handling for Fine Manipulation by Minimum D.O.F. Robotic Hand", *Proc. IEEE Int. Conf. on Robotics and Automation*, Orlando, Florida, pp.2454-2459, May, 2006.
- [22] T.McInerney and D.Terzopoulos, "Deformable Models in Medical Image Analysis: A survey", *Medical Image Analysis*, Vol.1, No.2, pp.91-108, 1996.
- [23] J.Cho and P.Benkeser, "Elastically Deformable Model-based Motion-Tracking of Left Ventricle", *Proc. IEEE Int. Conf. on Engineering in Medicine and Biology Society*, San Francisco, California, pp.1925-1928, Sept., 2004.
- [24] J.L.Johnson, "Contact Mechanics", Cambridge University Press, Chapter 4, 1985.
- [25] Y.Tatara, "On Compression of Rubber Elastic Sphere Over a Large Range of Displacements-Part I:Theoretical Study", *ASME Journal of Engineering Materials and Technology*, Vol.113, pp.285-291, 1991.
- [26] H.Goldstein, "Classical Mechanics (3rd)", Addison Wesley, 2002.
- [27] F.Amirouche: Computational Methods in Multibody Dynamics, *Prentice-Hall International Editions*, 1992.
- [28] J.Baumgarte: Stabilization of Constraints and Integrals of Motion in Dynamical Systems, *Computer Methods in Applied Mechanics and Engineering*, Vol.1, pp.1-16, 1972.

- [29] T.Park and E.Haug: A Hybrid Numerical Integration Method for Machine Dynamic Simulation, *ASME Trans. on Mechanisms, Transmissions, and Automation in Design*, Vol.108, pp.211-216, 1986.
- [30] J.Jalón and E.Bayo: Kinematic and Dynamic Simulation of Multibody Systems, *Springer Verlag*, Chaper 5, 1993.